

DRAFTS: A Deep, Rapid Archival Flare Transient Search in the Galactic Bulge

Rachel A. Osten

Space Telescope Science Institute, 3700 San Martin Drive, Baltimore, MD 21218

`osten@stsci.edu`

Adam Kowalski

Astronomy Department, Box 351580, University of Washington, Seattle, WA 98195

Kailash Sahu

Space Telescope Science Institute, 3700 San Martin Drive, Baltimore, MD 21218

Suzanne L. Hawley

Astronomy Department, Box 351580, University of Washington, Seattle, WA 98195

ABSTRACT

We utilize the Sagittarius Window Eclipsing Extrasolar Planet Search (SWEEPS) HST/ACS dataset for a Deep Rapid Archival Flare Transient Search (DRAFTS) to constrain the flare rate toward the older stellar population in the Galactic bulge. During 7 days of monitoring 229,293 stars brighter than $V=29.5$, we find evidence for flaring activity in 105 stars between $V=20$ and $V=28$. We divided the sample into non-variable stars and variable stars whose light curves contain large-scale variability. The flare rate on variable stars is ~ 700 times that of non-variable stars, with a significant correlation between the amount of underlying stellar variability and peak flare amplitude. The flare energy loss rates are generally higher than those of nearby well-studied single dMe flare stars. The distribution of proper motions is consistent with the flaring stars being at the distance and age of the Galactic bulge. If they are single dwarfs, they span a range of $\approx 1.0 - 0.25M_{\odot}$. A majority of the flaring stars exhibit periodic photometric modulations with $P < 3d$. If these are tidally locked magnetically active binary systems, their fraction in the bulge is enhanced by a factor of ~ 20 compared to the local value. These stars may be useful for placing constraints on the angular momentum evolution of cool close binary stars. Our results expand the type of stars studied for flares in the optical band, and suggest that future sensitive optical time-domain studies will have to contend with a larger sample of flaring stars than the M dwarf flare stars usually considered.

Subject headings: stars: activity — stars: flare — stars: late-type — stars: binaries: close

1. Introduction

Stellar flares are the most dramatic example of variability seen in stars with outer convective envelopes during the bulk of their lifetimes. The study of stellar flares can inform several topics: understanding the observable manifestations of magnetic reconnection in stellar atmospheres; constraining the expected stellar flare rate in optical transient searches for rare phenomena; and exploring the importance of stellar flares on exoplanet environment and habitability. The study of solar white-light flares has revealed the importance of the UV and optical regions in the energetics of flares; although flare variations at other wavelength regions such as X-rays are larger, white light continuum emission dominates the total radiated energy, by factors of roughly 100 with respect to X-ray energies (Emslie et al. 2005; Kretzschmar 2011).

The general consensus appears to be that stellar flares are produced by the same basic physical processes occurring in solar flares. This is despite the fact that flaring stars can be significantly different from the Sun: F dwarfs (Mullan & Mathioudakis 2000), G and K giants (Ayres et al. 1999, 2001; Testa et al. 2007), tidally locked RS CVn binary systems (Osten et al. 2004), dMe flare stars (Osten et al. 2005), flares on hyperactive young Suns containing star-disk interactions (Favata et al. 2005), and very low mass dwarfs near the substellar limit (Stelzer et al. 2006). At optical wavelengths, the selection for significant brightness increase in broad band filters means that M dwarfs are the primary observed flaring stars, due to the intrinsic red stellar spectrum compared with the blue flare spectrum (flare continua are characterized roughly by a blackbody of $T \sim 10^4$ K compared with stellar $T_{\text{eff}} \lesssim 3500$ K; Hawley et al. 2003). dMe stars are known to undergo dramatic optical variations (peak enhancements in the U band can be several magnitudes over timescales of minutes), with mean flare energies in the U-band of about 10^{32} erg — comparable to the largest solar flares. The flare rates for the most active dMe flare stars are 0.2–6 flares/star/hr, 10^4 – 10^5 times that for the Sun (Lacy et al. 1976). Optical flare timescales on M dwarf flare stars can range from less than a minute to several tens of minutes (Hawley et al. 2003) with mean flare duration independent of flare amplitude (Kunkel 1973).

Due to their dependence on the presence and dynamics of interacting magnetic fields, stellar flares are a diagnostic of transient magnetic activity, in addition to more commonly used persistent indicators such as chromospheric/coronal emissions, starspots and rotation. In situations where persistent magnetic activity is lacking, transient magnetic activity pro-

vides a complementary diagnostic of the presence of large-scale magnetic fields. Magnetic activity is a function of convection zone depth and rotation rate, as quantified by the Rossby number (Noyes et al. 1984), for stars that are not fully convective. This relates ultimately to the dynamo mechanism producing the large-scale magnetic fields whose stresses and plasma interactions cause the mechanical heating and reconnection observed as different magnetic activity phenomena. In single solar-like stars, magnetic activity is a function of age, with young stars exhibiting enhanced magnetic activity, and a consequent fall-off with increasing age accompanying spin-down (Skumanich 1972; Soderblom 1982). Likewise, the stellar flare rate appears to decline as a function of age. Results for low mass stars have suggested that activity timescales for fully convective stars may be as large as 10 Gyr (Delfosse et al. 1998; West et al. 2008). While there have been several recent studies concentrating on the flaring rate in young stars (Wolk et al. 2005; Stelzer et al. 2000), the decline in activity at Gyr ages means that relatively short exposures of single stars will generally not reveal any flaring activity, and the flare rate in older stars has not been studied systematically. Statistical studies of stellar magnetic activity have found that the flare rate decreases with height above the Galactic plane, as dynamical effects cause stars to move farther away from the plane as they age (Welsh et al. 2007; Kowalski et al. 2009; Hilton et al. 2010b; Walkowicz et al. 2011).

Stellar flares can also occur in binary systems. For tidally locked binaries, the tidal interaction forces the stars to rotate rapidly, in synchrony with the orbital period. Several classes of binary systems with at least one cool member are tidally locked (notably the RS CVn, BY Dra, and W UMa type binaries) and display enhanced chromospheric and coronal activity, and the RS CVn and BY Dra cases commonly demonstrate large individual flaring events (Guinan & Giménez 1993). Because the tidal interaction causes the stars to rotate much more rapidly than if they were single, activity (including flaring) can be maintained in much older systems than for single stars. Algol binary systems, in which some mass transfer is taking place, can also display magnetic activity; as the spectral types of the cool secondary are similar to those seen in the RS CVn binaries, it is understood that the magnetically active secondary star is the site of such activity (Guinan & Giménez 1993).

Recent results from searches for deep optical fast (<1 hr) transients have indicated the prevalence of stellar flaring and bolstered support for a better quantification of the flare rate. The three transients identified in Becker et al. (2004) turned out to be Galactic flare stars; Kulkarni & Rau (2006) described this population as a foreground “fog” potentially obscuring extragalactic fast optical transients (timescales of ≈ 1000 s). Fresneau et al. (2001) reported results from an astrographic plate survey at low galactic latitude, covering a large field of view (520 degrees²) at B magnitudes between 10 and 14; 8% of stars showed flare events greater than 0.4 mag over 20-30 minute timescales. Ramsay & Hakala (2005) performed sensitive but shallow temporal coverage observations at intermediate galactic latitude, reaching depths of

$V \sim 22.5$ on \sim minute timescales. With only 2 hours per field, they found 45 variable targets with 2 flare-like objects. From $V > 16.5$ mag to 22.5, $\approx 0.2\%$ of stellar sources were variable. This is especially problematic for sensitive transient searches like PanSTARRS and LSST, the latter possibly having as many as 50 stellar flares in each u band exposure (Hilton et al. 2010a).

On normal stars, we expect temporal variations in the stellar light to come from surface activity, as well as from eclipses by stellar or substellar companions and variations due to seismic waves from the stellar interior. Flares are stochastically occurring, and tend to have fast timescales, although large long-duration flares can last for hours. On the Sun, white-light flares have typical durations of only a few minutes, with small enhancements (>10 ppm; Kretzschmar 2011). A second source of temporal variations are due to the rotation of surface features on and off the stellar disk. Concentrations of surface magnetic field can produce intensity variations both lighter (such as faculae) and darker (such as spots) than the surrounding photospheric material: these features can be long-lived, producing regular photometric variations over multiple rotation periods if the size and location do not change appreciably during its lifetime (Hussain 2002). Irregular periodic variations could be due to growth and evolution of these surface features. Coupled with differential rotation of the stellar surface, these effects add complexity to the periodic variations beyond a simple sinusoidal dependence.

Because the flare rate is expected to be low on older stars, a systematic search for flares in an older stellar population needs a large number of stars, and involve a relatively long stare coupled with fast cadence to detect and resolve the flaring emission from any other variability. Sahu et al. (2006) announced the discovery of 16 candidate extrasolar planets using nearly continuous 7 day Hubble Space Telescope/Advanced Camera for Surveys (HST/ACS) monitoring of one field of 229,701 stars in two filters. The motivation for the initial study was to look for transiting extrasolar planets with lower masses and a larger range of metallicities in a part of the Galaxy that had not been explored previously. The color-magnitude diagram of the stars shows that the field is dominated by old stars associated with the Galactic bulge, as well as younger objects from the foreground disk population. The bulge population has an age estimated from isochrone fitting of ~ 10 Gyr. Due to the characteristics of the stellar target sample and observing strategy, this dataset is ideal for the purposes of studying the incidence of stellar flares in an older stellar population and comparing to the decline of magnetic activity seen in younger stellar populations, and thus forms the basis of the archival project described in this paper. The paper is laid out as follows: §2 summarizes the data reduction, §3 describes the analysis of the light curves, §4 describes the results, §5 discusses the implications, and §6 summarizes.

2. Data Reduction

The data used in this paper originally came from the SWEEPS project, described in Sahu et al. (2006). The SWEEPS field (202"×202") was imaged continuously for 7 days in 2004 February. The observations consist of 254 exposures in V (F606W) and 265 in I (F814W), each with an exposure time of 339 seconds, and typical spacing between individual observations ∼8 minutes. The time-series photometry was obtained through the use of difference imaging and is described in Sahu et al. (2006). For each star, a time series of relative intensities was constructed. Because the contrast of flares to the surrounding photosphere is highest at shorter wavelengths, we concentrate primarily on the *V* band time series in this paper. The magnitude and color of each star were used to estimate stellar parameters such as mass and temperature. The time series data are already calibrated and provide the starting point to examine evidence for variability and flares.

3. Analysis

The total number of stars in the SWEEPS sample brighter than $V=29.5$ is 229,293. After perusal of the light curves, a subset was retained where more than 70% of the light curve points have error bars no larger than three times the standard deviation. This reduced the number of stars to 222,657. A further cut was made on stars fainter than $V=20$ to select dwarf stars, reducing the number to 216,136. This serves as the starting point for our flare transient search, which we describe in more detail below.

3.1. Sample Division and Detrending of Variable Stars

The data format is a record of the relative flux of each star, where $V_{\text{rel},i}$ is the relative flux of the i th time bin, defined as

$$V_{\text{rel},i} = (\Delta F/F)_i = \left(\frac{F_i - \overline{F}}{\overline{F}} \right)_V \quad (1)$$

where F_i is the flux measured in time bin i , and \overline{F} is the average flux computed from the entire time series for a given filter (here, the V606W filter). $I_{\text{rel},i}$ is defined similarly for the F814W filter. The quantity $V_{\text{rel},i}$ is also expressed as $\Delta F/F_i$ in some figures in the paper. In order to characterize the light curves to search for transient variability, we determined a number of statistics. The first cut utilized the reduced chi-squared statistic of the relative flux summed over the time series. For these purposes χ^2_ν is defined as

$$\chi_\nu^2 = \frac{\sum_i V_{\text{rel},i}^2 / \sigma_i^2}{(N_{\text{lc}} - 1)} \quad (2)$$

where $V_{\text{rel},i}$ is defined above, σ_i is the uncertainty associated with the measurement, and N_{lc} is the number of points in the light curve. Stars with a reduced chi-squared less than 1.5 were termed non-variable, and those with $\chi_\nu^2 > 1.5$ variable. The numbers of non-variable and variable stars using this definition are 214,181 and 1955, respectively. Figure 1 displays the distribution of these two classes as a function of stellar V magnitude.

The variable star sample had underlying large-scale variations (large amplitude and long duration relative to single epochs), which needed to be removed in order to see any evidence of short-term flare variations. The following two approaches were applied to all light curves in the variable star sample, and the best fit was retained. In the first approach, periodic variations were identified using a Lomb normalized periodogram, and the light curve was folded to the dominant period. The light curve was then fit by a sum of up to 4 sine terms:

$$V_{\text{rel},i} = \sum_{n=1}^{\text{max1}} a_n \sin(2\pi n(\phi_i + \rho_n)) \quad (3)$$

where $V_{\text{rel},i}$ is the relative flux at epoch i , ϕ_i is the phase of epoch i when folded over the dominant period, ρ_n is a phase offset, and a_n is a normalization. The number of sine terms max1 was set to 2 or 4, following Pojmanski (2002). An F-test determined whether the additional two terms produced a statistically significant decrease in the chi-squared statistic. In the second approach, the light curves were fit by a sum of sines with up to 8 terms, using the following prescription:

$$V_{\text{rel},i} = \sum_{n=1}^{\text{max2}} a_n \sin(2\pi n(\tilde{t}_i + \rho_n)) \quad (4)$$

with \tilde{t} a normalized time ($\tilde{t}_i = t_i / (t_{\text{max}} - t_{\text{min}})$) where t_{max} and t_{min} are the last and first times in the time series, respectively, and max2 was 2, 4, 6, or 8, giving up to 16 free parameters. The value of max2 was taken to be larger than max1 to allow more flexibility with the irregularly variable stars. We performed fits to optimize the parameters. A decision as to which prescription (described by equation 3 or 4) was better was made by comparing χ^2 and number of degrees of freedom ν through an F-test. The fit was then subtracted from the original time series to detrend the light curve. We termed light curves fit better by the first approach regularly variable, and those described better by the second approach irregularly variable. A total of 1837 out of the 1955 variable objects had successful detrending. Of the 1955 variable objects, 1443 were regularly variable and 512 irregularly variable; the number changed to 1335 and 502, respectively, for the variable objects with successful detrending.

The majority of the regularly variable objects discarded due to poor detrending had very short (<0.4 d) periods. The first two panels of Figure 2 illustrate the detrending process for a regularly variable star, while the first two panels of Figure 3 illustrate the process for an irregularly variable star.

3.2. Flare Selection

We tested a couple of different statistics in developing our algorithm to find flares. Initially we used an $n\sigma$ cut, filtering on individual points which were outliers from $V_{\text{rel}} = 0$ at the level of $n\sigma$. With $n \gtrsim 5$ and σ the standard deviation of a normally distributed dataset, Gaussian statistics indicates a low probability of such events happening, and this method can be used to identify outliers which may be flares. However, there are potentially a large number of cosmic ray hits which may show up as outliers using this method, and while it is theoretically possible to separate a true flare which occurs in a single time bin from a cosmic ray by using the PSF shape of that exposure for that star, this method returns an unwieldy number of potential flares. We decided instead to employ a different set of criteria based on adjacent time bins. We define a statistic ϕ_{VV} based on the work of Welch & Stetson (1993) and Stetson (1996), as follows:

$$\phi_{VV} = \left(\frac{V_{\text{rel}}}{\sigma} \right)_i \times \left(\frac{V_{\text{rel}}}{\sigma} \right)_j \quad (5)$$

where $V_{\text{rel},i}$ is the relative flux in epoch i (after detrending, if necessary; see §3.1), and σ_i is the error on the measurement in epoch i . This computation is done for each subsequent pair of temporal data, so that $j = i + 1$. Whereas Welch & Stetson (1993) and Stetson (1996) developed this index to investigate variability in multi-band and multi-epoch photometry, the ϕ_{VV} statistic here is applied to subsequent epoch pairs in the same band in our database. A similar technique was used in the analysis of M dwarf flaring in the Sloan Digital Sky Survey Stripe 82 dataset discussed by Kowalski et al. (2009). In order to limit the number of false detections, we applied the false discovery rate analysis of Miller et al. (2001) to select flare candidate epochs by using a ϕ_{VV} threshold.

False-discovery rate analysis (Miller et al. 2001; Hopkins et al. 2002) allows us to set a critical threshold value of Φ_{VV} to select flare epochs while ensuring a given percentage of false-positives. The FDR technique has been recently employed for flare rate studies in Kowalski et al. (2009) and Hilton et al. (2010b), as well as other astrophysical applications. We begin by dividing the variable detrended (excluding those stars with poor detrending) star sample distribution of Φ_{VV} pairs (464,761 epoch pairs) into a null distribution (non-flaring epochs produced from spurious deviations in the data) and a candidate distribution

(a mix of real flares and spurious non-flares). For the purposes of this calculation we exclude from consideration epoch pairs in which $\Phi_{VV} > 0$ but the values of $V_{\text{rel},i,j} < 0$. Specifically, the null distribution is composed of the epoch-pairs consisting of a positive flux change in one epoch and a negative flux change in the other epoch (*i.e.*, negative values of Φ_{VV} ; 207,381 Φ_{VV} pairs). The null distributions for positive then negative flux changes was tallied separately from the distribution for negative then positive flux changes, to gauge similarity. The candidate distribution consists of the epoch pairs with a positive flux enhancement in both epochs (positive values of Φ_{VV} and $V_{\text{rel},i,j} > 0$; 130,117 Φ_{VV} pairs). The sum of these two numbers is smaller than the total number of epoch pairs due to exclusion of eclipses, which have a positive Φ_{VV} but are negative in both epochs. In Figure 4, we plot the absolute value of the nulls compared to the candidate distribution. The candidate distribution contains a significant tail that is not present in the nulls. Above our FDR-set threshold (see below), the number of spurious epochs divided by the number of total epochs (spurious epochs and real flares) is less than or equal to our pre-determined false-discovery rate, given by the variable α . The ratio of spurious epochs to total epochs using the null distribution comprised of negative then positive flux changes was 0.14, and for positive then negative flux changes it was 0.10.

For α , we choose 10%, based on experience with similar datasets in Kowalski et al. (2009). Successful FDR analysis requires a good understanding (model) of the null. We fit a double Gaussian to model the absolute value of the null distribution for the variable star sample (one Gaussian for $\Phi_{VV} < 5.38$, one for $\Phi_{VV} > 5.38$) for the Φ_{VV} range from 0 to 111 (the maximum value of Φ_{VV} in the candidate distribution). This was done to approximate the tail of the distribution which exhibited an apparent break near $\phi_{VV}=5.38$. From the double Gaussian, we calculate a p-value for each value of Φ_{VV} in the candidate distribution, where the p-value for a Φ_{VV} bin represents the probability that a null epoch-pair has that value of Φ_{VV} or greater. Then, given our pre-determined α , the FDR IDL prescription in Miller et al. (2001, ; Appendix B) sets the critical threshold. For $\alpha = 10\%$, the critical threshold is ~ 14.5 . This limits the candidate distribution from 130,117 epoch pairs with $\phi_{VV} > 0$ and $V_{\text{rel},i,j} > 0$ to 920 epoch pairs. We additionally apply the criterion that the flux divided by the standard deviation in the detrended light curve be > 2.5 in order to guard against light curves with marginal detrending. This limits our variable-star flare sample to 229 epoch pairs for by-eye inspection. We apply the same Φ_{VV} and standard deviation cuts to the non-variable star sample. The same distribution of null vs candidate epochs for the non-variable star sample is shown in Figure 4.

The bottom two panels of Figures 2 and 3 demonstrate the flare identification technique on variable stars, while Figure 5 demonstrates the process on a non-variable star. Out of 214,181 stars in the non-variable sample, 17 epoch pairs survived using this rigorous filtering.

In the variable star sample of 1837 stars, 229 epoch pairs were retained. The next step was to visually inspect all candidate flare epoch pairs. The above steps were done using V_{rel} , and we examined the variations in I_{rel} at this stage as well. We eliminated suspect flares, examples of which include flares occurring near times of particularly poor detrending (such as at the peak of a longer-lasting rise in intensity) or on light curves with very large scatter in general. This further reduced the number of candidate flare epochs. At this stage it became apparent that systematically the first, 42nd and 43rd epochs were showing up as flares, and we removed these as well. This leaves us with 16 epoch pairs on 16 stars in the non-variable light curves, and 106 flare events (128 flare detections) on the variable light curve sample (from 89 stars), for a total of 122 flares from 105 stars. Of the 89 variable stars exhibiting flares, 63 had regular periodic variations and 26 were irregularly variable. Table 1 gives a tabular breakdown of the flare identification process described above.

4. Results

4.1. The Nature of the Flares

Once the candidate flares were identified, we determined their properties. The flare selection described in the preceding section is primarily sensitive to the flare peaks, since that is where the signal is highest. In order to estimate flare properties such as total radiated energy and average flare luminosity, we considered points with $V_{\text{rel}} > 0$ on either side of the adjacent pair identified by the ϕ_{VV} statistic to define the flare duration. By the definition of the ϕ_{VV} statistic (see §3.2), each flare has a minimum of two points in it. Figure 6 illustrates some example flares.

We summed the intensities in the exposures identified as belonging to the flare and used the stellar luminosity to determine the flare energy in the F606W filter as follows:

$$E_{F606W} = L_{\star} \sum_i V_{\text{rel},i} \Delta t_i \quad (6)$$

where L_{\star} is the filter-specific stellar luminosity (determined from the color-magnitude diagram, assuming the star is at the mean bulge distance of 7.24 kpc; Clarkson et al. 2008), E_{F606W} is the integrated flare energy in the F606W filter, and Δt_i is the exposure time of the i th time bin in the flare, and $V_{\text{rel},i}$ is the relative flux in the F606W filter. We do not use photometric parallaxes from the color and apparent magnitude of the stars because of concerns about binarity; see §4.2. The zero point of the F606W filter was calculated as 2.87×10^{-9} erg $\text{cm}^{-2} \text{s}^{-1} \text{\AA}^{-1}$ using the flux calibrated spectrum of Vega (Bohlin 2007). Sequential V-band observations are 7.92 minutes apart (start time to start time), followed typically by a gap

due to spacecraft occultation; this leads to clumping in the histogram of elapsed times of the flare, going from 7.92 minutes to approximately 8 hours. The lower and upper values of the flare durations are 11 minutes and 33.9 minutes. Since we account only for the time when the star was observed in computing flare parameters, these derived quantities will be lower limits. The error on flare energy determination is estimated by adding in quadrature the statistical errors on each data point in the flare, and is typically $\sim 15\%$, independent of stellar magnitude. The light curve errors are reduced for brighter stars, but the flare contrast is also smaller for these stars. No error in the stellar quiescent luminosity L_\star is included explicitly, as the spread in distance modulus of stars in the SWEEPS field is $\sim \pm 1$ kpc from the mean bulge distance of 7.24 kpc (Clarkson et al. 2008), and any deviation of the star from the mean bulge isochrone (from which the luminosity is estimated) imparts additional uncertainties.

We considered the distributions of energies of the flares detected on non-variable and variable stars. Kowalski et al. (2009) demonstrated that the flare frequency distribution of a large number of stars at lower cadence is consistent with higher cadence observations of a single star. We calculate a cumulative flare frequency distribution by determining ν , given the number of flares observed with a minimum energy E , where $\nu = N/\tau$, N being the number of flares (106 and 16 for variable and non-variable stars, respectively) and τ the total monitoring time. The total monitoring time τ is calculated as

$$\tau = N_s T_{\text{mon}} \quad (7)$$

where N_s is the number of flaring stars considered in each category (89 and 16 for variable and non-variable samples, respectively), and T_{mon} is the monitoring time per star (for the V band data only, this is 0.9848 days when adding up exposures in this filter over the course of the 6.96 day observation). The flare frequency distribution can then be plotted as ν versus E , and the slope of the distribution determined from a fit to the trend in log space, using the functional form $\log \nu = \alpha + \beta \log E$ (Lacy et al. 1976). The top panel of Figure 7 shows the flare frequency distribution of variable and non-variable flaring stars in the F606W filter. The derived intercepts, and slopes and errors are listed in Table 2. The slopes are the same to within the uncertainties, although it is apparent that the distribution for DRAFTS variable stars extends to higher energies (by a factor of 8) and exhibits a turnover near $10^{33.5}$ erg. In order to facilitate comparison with other flare surveys, we convert from F606W to U band. We related the energy in the F606W band to that in the Johnson V band by the ratio of the FWHM of the two filters (850 Å and 2324 Å for V band and F606W, respectively), ignoring the fact that the central wavelength of the Johnson V filter lies blueward of F606W by ≈ 400 Å, then use the Lacy et al. (1976) relation between E_V and E_U ($E_U = 1.8 \times E_V$) to estimate the energy of the flares in the U band (assuming that the same relation established

for flares on M stars holds for these flares as well). The bottom plot of Figure 7 shows a comparison between the flare frequency distribution of the variable flaring stars in the DRAFTS sample with the nearby cool binary YY Gem. The flare frequency distribution is flatter for YY Gem than for the DRAFTS stars. Table 2 lists the slopes derived from flares on the two sub-groups of variable stars and non-variable stars and YY Gem.

For each flaring star, we calculate the average energy loss rate due to flares, by summing the radiated energy of all the detected flares for a given star, and dividing by the monitoring time. In general the errors on this derived quantity tracks the errors for the individual flare energies, except for the case of stars with multiple flares per star, where the error can be lower, about 10%. This is plotted in Figure 8 for the DRAFTS stars, as well as the dMe stars in Lacy et al. (1976). The stellar bolometric luminosity was determined by conversion using stellar V magnitude and the bulge isochrone of Sahu et al. (2006). The bolometric luminosity for the stars in the Lacy et al. (1976) sample was taken from Reid & Hawley (2005). An estimate of our detection limit is shown in blue for a flare consisting of two epochs at 3.8σ (chosen because of the cutoff value of $\phi_{VV} = 14.5$, $\sqrt{14.5} \approx 3.8$). The deviation per epoch was then used to estimate the limiting relative flux. The higher energy flares dominate the energy budget for high luminosity stars (Lacy et al. 1976). The trend of average energy loss rate versus stellar bolometric luminosity was computed for the ensemble of DRAFTS flaring stars, as well as the two sub-groups; these fits are also plotted in Figure 8 and tabulated in Table 2. Lacy et al. (1976) presented a strong trend of the average flare energy loss rate of dMe stars with quiescent U band luminosity, whereas here we find a trend with quiescent bolometric luminosity.

4.2. The Nature of the Flaring Stars

Table A1 in the Appendix lists the properties of the flaring stars. Of the 214,181 stars in the non-variable sample, 16 stars flared. Of the 1837 variable stars with successful detrending, 89 flared, giving a flaring rate among non-variable stars and variable stars of 0.007% and 4.8%, respectively. Thus, the frequency of flaring among the variable stars exceeds that among the non-variable stars by a factor of ≈ 700 . Variable stars also exhibit multiple flares per star (average of 1.25 flares per star), in contrast to the non-flaring stars, which only had one flare per star. We find that 71% of the flaring stars exhibited only one flare during the 7 day observing window. The remainder of the flaring stars showed multiple flares, with the largest at five flares per star.

We are limited by statistics for the faint stars in our sample. As indicated in Figure 1, past a V magnitude of about 25, the number of stars returned as variable drops by roughly

a factor of two compared to the brighter stars, and the number of non-variable stars in this same magnitude range increases by a similar factor compared to brighter stars. If we consider only stars brighter than $V=25$, the flare rate among variable and non-variable stars is 87/1374 (6.3%) and 4/94,053 (0.004%), respectively, and the flaring frequency amongst these brighter variable stars exceeds that of similarly bright non-variable stars by a factor of 1600. The non-variable stars tend to lie at the faint end, which suggests that the signal-to-noise of the data are limiting our ability to see underlying variations. These stars may be exhibiting variability at the same relative level as the brighter stars, but our ability to diagnose this is compromised due to statistics. Figure 9 displays the distribution of the relative flux at the peak of the flare against V magnitude. Flares with an increase in flux of a few percent to a few tens of percent can be found for the stars at the bright end of the sample, and the flux increase required for a flare identification becomes larger as the stars become intrinsically fainter. This is a reflection of the statistics needed to identify flares and other longer temporal trends, which are better constrained for the brighter stars in the sample.

There is a marked increase in the frequency of flaring amongst photometrically variable stars compared to the non-variable stars in our sample. Of the flaring stars brighter than $V=25$, 96% exhibit some kind of variability, as gauged by the χ^2_ν statistic. The bottom panel of Figure 9 quantifies this further, using the “range” of the flare light curve, taken as the difference between the values in the 95th and 5th percentile in the original light curve (before any detrending has taken place), and the peak flare amplitude for that star (Walkowicz et al. 2011). For stars with multiple flares, this represents the largest amplitude flare seen. The non-variable stars have both the highest range and the largest flare amplitude, both likely reflecting the lower signal-to-noise of these generally fainter objects.

Figure 10 displays the locus of the flaring stars on a color-magnitude diagram, along with the other stars in the SWEEPS field. In general the flaring stars lie near the bulge isochrone, but there are several outliers, and the flaring variable stars tend to lie systematically to the right of the bulge isochrone. This could be due to one of three factors: (1) young disk stars; (2) binary stars within the bulge; or (3) stars with an enhanced metallicity. The bulge field analyzed in this paper lies at low galactic latitude ($b=-2.65^\circ$), and so we may encounter a substantial fraction of young disk stars. Note that we cannot exclude an enhanced metallicity as an explanation for the offset of the flaring stars from the bulge isochrone, but we can examine the other two possibilities.

We make use of the results of Clarkson et al. (2008), who computed stellar proper motions for the stars in this field using a second epoch of data in 2006. They were able to measure proper motions for more than 180,000 objects, and kinematically separate bulge

stars from disk stars. They determined that the fraction of disk stars in the SWEEPS field is approximately 14% for stars brighter than $I \sim 24$. Of the 105 flaring stars identified in the current paper, proper motions are available for 83/89 variable stars and 14/16 non-variable stars. Figure 11 shows the distribution of proper motions for the flaring stars, as well as a random distribution of 20,000 stars in the SWEEPS field. The flare star distribution is very similar to the general distribution of stars in the SWEEPS field, with no preference for being in the disk. The proper motion constraints are consistent with the flaring stars being at the distance of the bulge.

Because a large fraction of the flares detected occurred on variable stars (89 out of 105 stars), we investigated further the properties of the underlying variability. Of the 89 variable stars, 63 exhibited regular periodic variations. We note that the periods are returned from an automatic fitting of the light curves; they correspond to the peak frequency of the Lomb Normalized Periodogram and are used in a utilitarian manner in §3.1 to detrend the light curves. This analysis doesn’t examine whether the period is significant, nor does it attempt to address biases which can creep into periodogram analyses (e.g. from red noise or period aliasing). Also note that irregularly variable stars may have photometric periods which are statistically significant; the detrending process in section 3.1 concentrates on which of the two methods (given by equations 3 and 4, respectively) can better detrend the light curves. A plot of the period distribution of the flaring stars which exhibit regular variations shows that 53 out of 63 have periods $\lesssim 3$ days (Figure 12). This is $\approx 1/2$ the monitoring time of 6.96 days and may explain the apparent drop-off in the period distribution past 3 days. We note that three objects have apparent photometric periods in excess of the 6.96 day monitoring time, and are likely spurious. We concentrate on the objects having photometric periods less than 3 days as these are likely the most reliable, but they are subject to the caveats described above. Regular modulation at these timescales (for those less than about 3 days) may be due to rapid rotation of spotted young single stars. However, the proper motion constraints appear to rule this out. Another possibility is that of magnetically active (spotted) binaries (e.g. RS CVn, BY Dra, or W UMa binaries). Most of the signposts of youth (fast rotation, enhanced magnetic activity as evidenced by $H\alpha$ emission, X-ray emission, starspots, flaring) are also present in active binaries, as the tidal locking enforces fast rotation and consequent magnetic activity signatures at old age. Note that active binaries are typically detected via their enhanced chromospheric and/or X-ray emission in old stellar populations in globular clusters and old open clusters (Bassa et al. 2004; van den Berg et al. 2004; Kashyap et al. 2006), so if tidally locked, the stars could still be at the distance and age of the bulge population. As the binary fraction in the bulge is uncertain (Clarkson et al. 2008), and the proper motion measurements seem to indicate that the flaring stars are bulge members, the scenario that these flaring stars are detached magnetically active binaries is

likely. Spectroscopic observations would be needed to confirm or refute the binary nature of the flaring stars in favor of youth.

We can estimate the number of active binaries expected in this field from the disk, using the formalism of Tinney et al. (1993), as discussed in Koenig et al. (2008). We calculate an effective volume V_{eff} which takes into account spatial inhomogeneities probed by our sight-line, using an exponential fall-off with increasing distance from the galactic plane. This V_{eff} is

$$V_{\text{eff}} = \Omega \left(\frac{h}{\sin |b|} \right)^3 [2 - (\xi^2 + 2\xi + 2) * \exp(-\xi)], \quad (8)$$

where $\xi = d \sin |b|/h$, h is the exponential scale height, $|b|$ the absolute value of the galactic latitude of the pointing (here 2.65°), Ω the solid angle subtended by the $202'' \times 202''$ arcsec field of view of the ACS observations, and d is the mean-bulge distance, taken to be 7.24 kpc (from Clarkson et al. 2008). We use the space density of active binaries from near-field measurements, with $n_{AB} = 3.7 \times 10^{-5}$ stars pc^{-3} (Favata et al. 1995) to determine the number of active binaries from the disk we would expect to see, using $N_{AB} = n_{AB} V_{\text{eff}}$, and find that N_{AB} is between 1 and 2. This calculation shows that the expected number of disk active binaries is low, and cannot account for the total number of flaring objects, consistent with other constraints suggesting the bulge nature of the DRAFTS binaries.

Under the assumption that the variable flaring stars in our sample are all active binaries, we can take a uniform distribution through the volume of the bulge sampled in this exposure to constrain the space density of active binaries in the bulge. According to Clarkson et al. (2008) the spread in distance modulus of the SWEPS field is about 1 kpc from the mean bulge distance of 7.24 kpc. For a volume using the field of view translated into distance at the near and far end of this distance spread and height of 2 kpc, we calculate a space density of active binaries of 8.8×10^{-4} stars pc^{-3} , or an enhancement of roughly 20 compared to the value found locally by Favata et al. (1995). The disparity between the elapsed time covered in the study (6.95 days) and the monitoring time per star in the F606W band (0.98 days) may have led us to miss flaring behavior on other variable stars if the flares occurred during occultations or I814W observations. The number of variable stars is roughly a factor of 20 larger than the subset of flaring variable stars, so this explanation would not account for all variable stars having flares within a seven day period. It does suggest that the enhancement of roughly 20 in the space density of active binaries in the bulge compared to the local value may be a lower limit. Stellar densities are expected to be higher in the bulge compared to the value locally, and this may lead to an enhancement in the binary fraction. The study presented in this paper, while not specifically tuned to finding binaries, may be an indirect way to detect the presence of magnetically active binaries through sensitive flare searches and thus place a quantitative constraint on binary fraction in stellar associations like the

Galactic bulge and old open clusters.

5. Discussion

The sample of stars surveyed for flares in this paper is markedly different from the types of stars and wavelength ranges usually surveyed for stellar flares. Because of the large amount of contrast with underlying coronal emission and the impulsive nature of flares, many studies of flares have concentrated on the high energy (extreme ultraviolet to X-ray) region (Wolk et al. 2005; Stelzer et al. 2000; Audard et al. 2000; Osten & Brown 1999) to characterize flares on young stars, active stars and binaries. Due to the intrinsically red light of M stars in quiescence, their blue flares are easily studied in the optical (Lacy et al. 1976; Kowalski et al. 2009; Hilton et al. 2010b). More recently, the long stellar time series returned by the Kepler mission have been explored in the context of white light flares on stars later than K0 spectral type (Walkowicz et al. 2011) for long duration flares lasting more than 1.5 hours. The high energy measurements have been flux- and therefore distance-limited, and the optical flare studies have preferentially focused on younger stars, due to the known decline of magnetic activity and flaring with age (and the correlation between stellar age and increasing distance from the Galactic plane). This study is the first to cover a wide range of cool stellar spectral types at optical wavelengths, while sampling an older population of stars.

Our supposition is that our sample of flaring bulge stars is dominated by a population of cool close binaries displaying magnetic activity through transient flaring activity. The magnetic activity of such close binaries is usually studied through their coronal and chromospheric time-averaged properties; multi-wavelength flare campaigns to study the properties of flares on solar neighborhood binaries (Stern et al. 1992; Osten et al. 2002, 2004) have concentrated on ultraviolet, X-ray, and radio measurements. As discussed by Henry & Newsom (1996), there are very few observations of optical flaring on nearby active detached binaries with G and K primaries – by far the most attention has been on optical studies of late K/M dwarf binaries such as YY Gem (Doyle & Mathioudakis 1990). One notable exception is a large optical flare on the binary HR 1099 (K1IV+G5V) observed by both Zhang et al. (1990) and Henry & Hall (1991), with peak enhancements noted in the V band (at different times) of 0.18 and 0.42 magnitudes, respectively. Mathioudakis et al. (1992) and Henry & Newsom (1996) determined the optical flare rate for the nearby active binary II Peg (K2 IV+dM) to be near $0.2 \text{ flares hr}^{-1}$ using different data sets, although Henry & Newsom (1996) noted variation in the flare rate. Rucinski (1985) and references therein mention that a few flares have been seen in contact binaries of the W UMa type (containing magnetically active stars),

and they appear to follow the relations of M dwarf flare stars. Such observations do not generally suffice to compute a flare frequency distribution with energy or other flare statistics to which we can compare our results, and so we instead look to the statistics on optical M dwarf flares for comparison.

As noted in §4.1, the flare frequency distributions of the non-variable and variable DRAFTS stars contain several notable differences. The DRAFTS variable flaring stars have both more numerous and more energetic flares than the non-variable flaring stars, with maximum energy roughly a factor of 10 larger. The slopes of the distributions are similar to within the uncertainties, however the most energetic flares on the DRAFTS variable flaring stars have a much steeper slope of -2.68 above $10^{33.5}$ erg (see Table 2.) The bottom panel of Figure 7 compares the flare frequency distribution with energy of the ensemble of stellar flares from DRAFTS variable stars against that determined by Lacy et al. (1976) for optical flares on the M dwarf binary YY Gem. This binary, composed of two M1 stars (Strassmeier 2009) was chosen because of its general level of enhanced magnetic activity, as evidenced by starspots, chromospheric and coronal emission, and a high flaring rate. It also has the advantage of being relatively well-observed in its flare properties. The largest stellar flare energies from YY Gem and the DRAFTS variable flare stars are similar, assuming that the same conversion applies; the study of YY Gem is clearly sensitive to lower energy events. The distribution of flares with energy for YY Gem has an apparent break around $10^{33.5}$ erg, which is also near where the distribution of flare energies in the DRAFTS variable stars shows evidence of a rollover. Table 2 shows the slopes of the distributions computed for this high energy end. The DRAFTS flaring variable stars show a much steeper trend. The few optical flares seen on nearby active binaries have exhibited flare energies that can approach 10^6 times the largest solar flare energies of 10^{32} ergs (Henry & Hall 1991), although the evolved nature of the flaring binary member(s) may play a role in these extremes. Doyle & Mathioudakis (1990) noted that the binary nature of YY Gem may be responsible for the change in the flare frequency distribution above $10^{33.5}$ erg, as the increased volumes allow for more energy to be stored and released during flares. Figure 8 plots the average energy loss rate due to flares for the flaring stars in our sample and the sample of M dwarf flare stars studied by Lacy et al. (1976). YY Gem has the highest average energy loss rate of the dMe stars considered in Lacy et al. (1976). It even exceeds the DRAFTS stars at the same total light. Ferreira (1998) pointed out that such energetic flares in cool binaries require strong magnetic fields on at least one of the stars, and possibly also a large volume.

Lacy et al. (1976) found that the luminous M dwarfs emit more energy in flares than the faint M dwarfs, even when one accounts for the smaller “flare visibility” on the more luminous stars. We find that the energy loss rate of the non-variable stars tends to be smaller than variable stars, even taking into account the general faintness of the former compared

with latter, which biases our flare detection to larger flare events (fits to the subsets and the entire set of DRAFTS flaring stars are given in Table 2). This confirms the results shown in Figure 7 which demonstrate more frequent and energetic flaring for the DRAFTS variable flare stars. The dMe stars in Lacy et al. (1976) show a steeper trend of flare energy loss rate vs. luminosity than the DRAFTS flaring stars in Figure 8, even though the average energy loss rate of the DRAFTS flaring stars can be up to 30 times higher. The energy loss rate of these trends at the solar value suggests roughly an order of magnitude higher flare energy loss rate for the dMe stars than for the DRAFTS flaring stars. It is thought that the relation for M dwarfs turns over at spectral type dK since even the largest solar flares are much weaker than what an extrapolation predicts. Possibilities for the different slopes may arise from the different internal structures of the dMe stars considered in Lacy et al. (1976) compared to the higher luminosity/mass DRAFTS flaring stars, or the hypothesized binary nature of the DRAFTS variable stars. We note that the one dMe star in that sample which is a close binary is YY Gem, whose average flare energy loss rate is in the range of the DRAFTS flaring stars. If the bulk of the DRAFTS flaring stars are indeed binaries, this would shift the $L_{\text{bol}}/L_{\text{sun}}$ values for DRAFTS flaring stars in Figure 8 to the left, and bring the values into better agreement with YY Gem.

Overall, only a small fraction of stars in the sample flare, but their flare rates are large by comparison with measures of flaring in other kinds of active stars. The 105 flaring stars represent 0.05% of all the bulge stars searched for flares, taking the 14% disk fraction of Clarkson et al. (2008) and the number of stars with $V > 20$. Figure 13 shows the variation of flaring fraction versus stellar magnitude for the stars exhibiting underlying variability. For each magnitude bin, the number of flaring epochs was divided by the number of total epochs in that magnitude bin. Kowalski et al. (2009) found a maximum flare rate of M dwarfs near the galactic plane (at $b \sim -38^\circ$) for flares with $\Delta u > 0.7$ mag on stars with $u < 22$ of 8 flares $\text{hr}^{-1} \text{ deg}^{-2}$. The flaring stars in the Kepler field studied by Walkowicz et al. (2011) were of spectral type K0V and cooler, and had much smaller peak amplitudes, at $\Delta F/F > 0.1\%$ generally, but represent an approximate flaring rate of 0.03 flares $\text{hr}^{-1} \text{ deg}^{-2}$ (this number may actually be higher, even for the stellar range considered in the paper, since only a subset of stars in the 105 degree² Kepler field are selected for monitoring). We compute the spatial flare rate for the DRAFTS flaring stars using the effective monitoring time of the dataset (0.9848 days) and solid angle subtended by the field of view, 0.003148 deg², which for 122 flares results in a flare rate of 1700 flares $\text{hr}^{-1} \text{ deg}^{-2}$, two orders of magnitude greater than that found by Kowalski et al. (2009). The bulge is of course a much more crowded field than any Galactic disk field, with an intrinsically larger number of stars per square degree, which will contribute to this enhancement. With sensitive photometry, this study is able to pick out much smaller flares on a larger variety of cool stars, with peak flare amplitudes as

small as a few percent, which may partly explain the much higher flare rate. The flare rate from this study can also be expressed as 1.2 flares per flaring star per day, which is about ten times higher than the X-ray flare rate of 0.13 flares per flaring star per day Wolk et al. (2005) determined on young single Suns in the Orion Nebula Cluster. Osten & Brown (1999) determined the extreme ultraviolet flare rate among a sample of nearby active binary systems to be in the range 0.1-1.5 flares per day, or 0.3 flares per day taking the entire flare sample as one. The DRAFTS flare rate is consistent with the upper end of this distribution, suggesting that the high precision of this optical study may balance the higher contrast in the extreme ultraviolet wavelength observations. These statistics demonstrate that the flaring stars found in this study exhibit flaring activity at the extremes found in magnetically active stars. This is also supported by the frequency distributions, comparable to one of the most energetic nearby flare stars, as well as by the increased average flare energy loss rate compared to most well-studied nearby M dwarf flare stars.

The high flaring rate has implications for current and future time-domain studies: given the derived spatial flare rate of $1700 \text{ flares hr}^{-1} \text{ deg}^{-2}$, a single 15 second frame of an exposure with the Large Synoptic Survey Telescope (LSST) ¹ covering 9.6 deg^2 might return as many as 68 flares with amplitudes greater than 1% of the quiescent luminosity. This is the same order as the maximum of 50 flares per LSST exposure from M dwarfs at low galactic latitudes with flares exceeding $\Delta u > 0.1 \text{ mag}$ (Hilton et al. 2010a), and suggests an underestimate of the contribution to the variable sky from flaring cool stars.

The existence of flaring in these old stars opens up other questions regarding the longevity of binary systems at this age. The traditional assumption about a decline of magnetic activity and flaring with stellar age arises mainly from consideration of single stars (Skumanich 1972; Soderblom 1982). For stars in a binary system close enough to have tidal interactions, tidal effects can cause synchronous rotation, circularizing the orbit and coupling the stars’ rotation to the orbit. This enforces fast rotation at old age, as discussed earlier. The synchronization time for stars with convective envelopes is relatively short, approximately 1 MY for near-unity mass ratios and orbital periods less than 3 days (Zahn 1977), and a binary with an orbital period < 3 days would circularize in about 1 GY. One can ask, though, how long such binaries can be maintained against angular momentum loss, particularly in the present case where we may be seeing flares from 10 GY binaries. The spin-orbit coupling which leads to enhanced magnetic activity can also result in orbital evolution of the system. Whereas in a single star, magnetic torques in a stellar wind lead to angular momentum loss and subsequent spin-down with time, in a close binary the coupling of the spin and

¹More information can be found at <http://www.lsst.org>.

orbital angular momenta paradoxically leads the angular momentum loss from the stellar wind to result in orbital shrinkage and associated faster rotation (Guinan & Giménez 1993). The exact timescale is given by the binary mass ratio, the initial period, and the nature of the stellar wind and its effect on magnetic braking. The angular momentum evolution of cool close binaries has been studied quantitatively (Guinan & Giménez 1993; Stepień 2011), using stellar wind/velocity variations with time found for single stars. Differences in these two treatments, which stem from different parameterizations of the angular momentum loss, can lead to differences in the timescales for evolution of a cool close binary to the contact stage or Roche Lobe overflow of up to an order of magnitude.

The evolution of close binaries in the bulge could also be affected by the higher number densities of stars in the bulge: a tertiary can affect the angular momentum evolution of close binaries through Kozai cycles accompanied by tidal friction (Fabrycky & Tremaine 2007). Another possibility for these stars, if spectroscopic confirmation shows that some of these are single, is that they are magnetically young (by virtue of their flaring and fast rotation) but kinematically old. They would then be similar to some solar neighborhood chromospherically young, kinematically old stars studied by Poveda et al. (1996) and Rocha-Pinto et al. (2002), and a plausible explanation for their existence at such old ages would be binary coalescence of a low mass, short period binary system into an apparently single, rapidly rotating (and flaring) star. Thus, while we do not know the exact nature of the stars in our sample, their activity (as deduced by the flares detected on them) and their 10 GY age (from proper motions consistent with the bulge) coupled with the few day periods observed from the data suggest that they may be able to place constraints on the angular momentum evolution of binary stars, if they are close binaries, or signal the formation timescales and coalescence rates of low mass stellar mergers.

6. Summary and Conclusions

We repurposed the Sagittarius Window Eclipsing Extrasolar Planet Search into a Deep Rapid Archival Flare Transient Search. Data from the nearly 7 day stare, coupled with rigorous tests to select candidate flare events, allowed us to identify 122 flares on 105 stars, out of a total of 216,136 stars surveyed. The characteristics of the flares are similar to those of optical flares on well-studied, nearby flaring stars, and suggest a high flaring rate. Stars with underlying variability produced flares at a higher rate than stars with no discernible variability, by a factor of nearly 700; this factor is 1600 when considering stars between $V=20$ and $V=25$. We interpret these underlying variations as arising from rotational modulation due to starspots. The flaring stars appear to be characterized by an older stellar population

which is likely binary in nature, and demonstrates the capability of tidally locked systems to retain magnetic activity in old age. The study expands the type of stars studied for flares in the optical band, and suggests that future optical time-domain studies will have to contend with a larger sample of potential flaring stars than the M dwarf flare stars usually considered. A more in-depth study of the nature of the variable flaring stars in the present sample will provide constraints on the nature of angular momentum evolution in old cool, magnetically active binary stars.

Based on data taken with the NASA/ESA Hubble Space Telescope obtained at the Space Telescope Science Institute (STScI). Support for this research was provided by NASA through grants AR-17767.0 and AR-17767.1 from STScI, which is operated by the Association of Universities for Research in Astronomy (AURA), inc., under NASA contract NAS5-26555. AFK and SLH acknowledge support from NSF grant 08-07205. We thank A. C. Becker, E. J. Hilton, and B. P. Brown for useful discussions. We also thank J. R. A. Davenport for the use of his contour routine.

REFERENCES

- Audard, M., Güdel, M., Drake, J. J., & Kashyap, V. L. 2000, *ApJ*, 541, 396
- Ayres, T. R., Osten, R. A., & Brown, A. 1999, *ApJ*, 526, 445
- . 2001, *ApJ*, 562, L83
- Bassa, C., Pooley, D., Homer, L., Verbunt, F., Gaensler, B. M., Lewin, W. H. G., Anderson, S. F., Margon, B., Kaspi, V. M., & van der Klis, M. 2004, *ApJ*, 609, 755
- Becker, A. C., Wittman, D. M., Boeshaar, P. C., Clocchiatti, A., Dell’Antonio, I. P., Frail, D. A., Halpern, J., Margoniner, V. E., Norman, D., Tyson, J. A., & Schommer, R. A. 2004, *ApJ*, 611, 418
- Bohlin, R. C. 2007, in *Astronomical Society of the Pacific Conference Series*, Vol. 364, *The Future of Photometric, Spectrophotometric and Polarimetric Standardization*, ed. C. Sterken, 315
- Clarkson, W., Sahu, K., Anderson, J., Smith, T. E., Brown, T. M., Rich, R. M., Casertano, S., Bond, H. E., Livio, M., Minniti, D., Panagia, N., Renzini, A., Valenti, J., & Zoccali, M. 2008, *ApJ*, 684, 1110
- Delfosse, X., Forveille, T., Perrier, C., & Mayor, M. 1998, *A&A*, 331, 581

- Doyle, J. G. & Mathioudakis, M. 1990, *A&A*, 227, 130
- Emslie, A. G., Dennis, B. R., Holman, G. D., & Hudson, H. S. 2005, *Journal of Geophysical Research (Space Physics)*, 110, A11103
- Fabrycky, D., & Tremaine, S. 2007, *ApJ*, 669, 1298
- Favata, F., Flaccomio, E., Reale, F., Micela, G., Sciortino, S., Shang, H., Stassun, K. G., & Feigelson, E. D. 2005, *ApJS*, 160, 469
- Favata, F., Micela, G., & Sciortino, S. 1995, *A&A*, 298, 482
- Ferreira, J. M. 1998, *A&A*, 335, 248
- Fresneau, A., Argyle, R. W., Marino, G., & Messina, S. 2001, *AJ*, 121, 517
- Guinan, E. F. & Giménez, A. 1993, in *Astrophysics and Space Science Library*, Vol. 177, *Astrophysics and Space Science Library*, ed. J. Sahade, G. E. McCluskey Jr., & Y. Kondo, 51–110
- Hawley, S. L., Allred, J. C., Johns-Krull, C. M., Fisher, G. H., Abbett, W. P., Alekseev, I., Avgoloupis, S. I., Deustua, S. E., Gunn, A., Seiradakis, J. H., Sirk, M. M., & Valenti, J. A. 2003, *ApJ*, 597, 535
- Henry, G. W. & Hall, D. S. 1991, *ApJ*, 373, L9
- Henry, G. W. & Newsom, M. S. 1996, *PASP*, 108, 242
- Hilton, E. J., Hawley, S. L., Kowalski, A. F., & Holtzman, J. 2010a, *ArXiv e-prints*
- Hilton, E. J., West, A. A., Hawley, S. L., & Kowalski, A. F. 2010b, *AJ*, 140, 1402
- Hopkins, A. M., Miller, C. J., Connolly, A. J., Genovese, C., Nichol, R. C., & Wasserman, L. 2002, *AJ*, 123, 1086
- Hussain, G. A. J. 2002, *Astronomische Nachrichten*, 323, 349
- Kashyap, V., Edmonds, P., Heinke, C., & Gilliland, R. 2006, in *Bulletin of the American Astronomical Society*, Vol. 38, *AAS/High Energy Astrophysics Division #9*, 338
- Koenig, X., Grindlay, J. E., van den Berg, M., Laycock, S., Zhao, P., Hong, J., & Schlegel, E. M. 2008, *ApJ*, 685, 463
- Kowalski, A. F., Hawley, S. L., Hilton, E. J., Becker, A. C., West, A. A., Bochanski, J. J., & Sesar, B. 2009, *AJ*, 138, 633

- Kretzschmar, M. 2011, *A&A*, 530, 84
- Kulkarni, S. R. & Rau, A. 2006, *ApJ*, 644, L63
- Kunkel, W. E. 1973, *ApJS*, 25, 1
- Lacy, C. H., Moffett, T. J., & Evans, D. S. 1976, *ApJS*, 30, 85
- Mathioudakis, M., Doyle, J. G., Avgoloupis, V., Mavridis, L. N., & Seiradakis, J. H. 1992, *MNRAS*, 255, 48
- Miller, C. J., Genovese, C., Nichol, R. C., Wasserman, L., Connolly, A., Reichart, D., Hopkins, A., Schneider, J., & Moore, A. 2001, *AJ*, 122, 3492
- Mullan, D. J. & Mathioudakis, M. 2000, *ApJ*, 544, 475
- Noyes, R. W., Weiss, N. O., & Vaughan, A. H. 1984, *ApJ*, 287, 769
- Osten, R. A. & Brown, A. 1999, *ApJ*, 515, 746
- Osten, R. A., Brown, A., Ayres, T. R., Drake, S. A., Franciosini, E., Pallavicini, R., Tagliaferri, G., Stewart, R. T., Skinner, S. L., & Linsky, J. L. 2004, *ApJS*, 153, 317
- Osten, R. A., Brown, A., Wood, B. E., & Brady, P. 2002, *ApJS*, 138, 99
- Osten, R. A., Hawley, S. L., Allred, J. C., Johns-Krull, C. M., & Roark, C. 2005, *ApJ*, 621, 398
- Pojmanski, G. 2002, *Acta Astron.*, 52, 397
- Poveda, A., Allen, C., Herrera, M. A., Cordero, G., & Lavalley, C. 1996, *A&A*, 308, 55
- Ramsay, G. & Hakala, P. 2005, *MNRAS*, 360, 314
- Reid, I. N. & Hawley, S. L. 2005, *New light on dark stars : red dwarfs, low-mass stars, brown dwarfs* (Springer-Praxis)
- Rocha-Pinto, H. J., Castilho, B. V., & Maciel, W. J. 2002, *A&A*, 384, 912
- Rucinski, S. M. 1985, in *NATO ASIC Proc. 150: Interacting Binaries*, ed. P. P. Eggleton & J. E. Pringle, 13–49
- Sahu, K. C., Casertano, S., Bond, H. E., Valenti, J., Ed Smith, T., Minniti, D., Zoccali, M., Livio, M., Panagia, N., Piskunov, N., Brown, T. M., Brown, T., Renzini, A., Rich, R. M., Clarkson, W., & Lubow, S. 2006, *Nature*, 443, 534

- Skumanich, A. 1972, *ApJ*, 171, 565
- Soderblom, D. R. 1982, *ApJ*, 263, 239
- Stępień, K. 2011, *Acta Astron.*, 61, 139
- Stelzer, B., Neuhauser, R., & Hambaryan, V. 2000, *A&A*, 356, 949
- Stelzer, B., Schmitt, J. H. M. M., Micela, G., & Liefke, C. 2006, *A&A*, 460, L35
- Stern, R. A., Uchida, Y., Walter, F., Vilhu, O., Hannikainen, D., Brown, A., Veale, A., & Haisch, B. M. 1992, *ApJ*, 391, 760
- Stetson, P. B. 1996, *PASP*, 108, 851
- Strassmeier, K. G. 2009, *A&A Rev.*, 17, 251
- Testa, P., Reale, F., Garcia-Alvarez, D., & Huenemoerder, D. P. 2007, *ApJ*, 663, 1232
- Tinney, C. G., Reid, I. N., & Mould, J. R. 1993, *ApJ*, 414, 254
- van den Berg, M., Tagliaferri, G., Belloni, T., & Verbunt, F. 2004, *A&A*, 418, 509
- Walkowicz, L. M., Basri, G., Batalha, N., Gilliland, R. L., Jenkins, J., Borucki, W. J., Koch, D., Caldwell, D., Dupree, A. K., Latham, D. W., Meibom, S., Howell, S., Brown, T. M., & Bryson, S. 2011, *AJ*, 141, 50
- Welch, D. L. & Stetson, P. B. 1993, *AJ*, 105, 1813
- Welsh, B. Y., Wheatley, J. M., Seibert, M., Browne, S. E., West, A. A., Siegmund, O. H. W., Barlow, T. A., Forster, K., Friedman, P. G., Martin, D. C., Morrissey, P., Small, T., Wyder, T., Schiminovich, D., Neff, S., & Rich, R. M. 2007, *ApJS*, 173, 673
- West, A. A., Hawley, S. L., Bochanski, J. J., Covey, K. R., Reid, I. N., Dhital, S., Hilton, E. J., & Masuda, M. 2008, *AJ*, 135, 785
- Wolk, S. J., Harnden, Jr., F. R., Flaccomio, E., Micela, G., Favata, F., Shang, H., & Feigelson, E. D. 2005, *ApJS*, 160, 423
- Zahn, J.-P. 1977, *A&A*, 57, 383
- Zhang, R.-X., Zhai, D.-S., Zhang, X.-B., Zhang, J.-T., & Li, Q.-S. 1990, *Information Bulletin on Variable Stars*, 3456, 1

7. Appendix

Table A1 lists the properties of the DRAFTS flaring stars: their positions, magnitudes in the F606W and I814W filters, the type of variability, the period of any underlying regular variability, and the range of the amplitude.

Table 1. DRAFTS Flare Search Breakdown

Selection Criterion	# in Variable Sample	# in Non-Variable Sample
Stars in the field		229,701
Stars with $V < 29.5$		229,293
Stars in which $>70\%$ of light curve bins have errors $< 3 \sigma$		222,657
Stars with $V > 20$		216,136
$\chi^2_\nu < 1.5$ (non-variable) or $\chi^2_\nu > 1.5$ (variable)	1955	214,181
Variable stars with successful detrending	1837	–
Epoch pairs with $\phi_{VV} > 14.5$, $V_{\text{rel},i,j} > 0$ ($j = i + 1$)	920	17
Epoch pairs with $V_{\text{rel},i}/\sigma_i > 2.5$	229	17
Individual flare detections	128	16
# flare events	106	16
Total # of flaring events		122
Flaring stars	89	16
Total # of flaring stars		105

Table 2. Flare Frequency Distributions

Category	Band	Intercept	Slope
$\log \nu = \alpha + \beta \log E$			
DRAFTS variable stars	F606W	46.1	-1.43±0.14 (N=106)
DRAFTS non-variable stars	F606W	57.8	-1.81±0.45 (N=16)
DRAFTS variable stars	U band	45.8	-1.43±0.14 (N=106)
YY Gem	U band	14.5	-0.49±0.12 (N=18)
DRAFTS variable stars, $E_{U,fl} > 10^{33.5}$ erg	88.1 U band		-2.68±0.49 (N=30)
YY Gem, $E_{U,fl} > 10^{33.5}$ erg	U band	55.5	-1.69±0.69 (N=6)
$\log E_{\text{tot,U}}/T_{\text{mon}} = \alpha + \beta \log L_{\text{bol}}/L_{\odot}$			
DRAFTS all stars	U band	28.7	0.59±0.04 (N=122)
DRAFTS variable stars	U band	28.7	0.53±0.05 (N=106)
DRAFTS non-variable stars	U band	28.2	0.33±0.04 (N=16)
Lacy et al. (1976) sample	U band	29.6	1.30±0.12 (N=8)

Table A1. Properties of DRAFTS Flaring Stars

RA (J2000)	Dec (J2000)	V (F606W)	I) (F814W)	Variability Type	Period (d)	Range ^a
17 58 53.38	-29 11 52.58	25.49	22.96	flat	...	0.30
17 58 54.29	-29 10 26.85	20.94	19.63	flat	...	0.02
17 58 54.38	-29 13 25.05	22.90	21.51	flat	...	0.05
17 59 0.37	-29 12 6.01	25.15	23.30	flat	...	0.26
17 58 59.43	-29 10 24.00	27.99	25.22	flat	...	2.51
17 58 53.98	-29 10 27.79	25.50	23.20	flat	...	0.37
17 58 53.54	-29 12 7.09	27.55	25.78	flat	...	1.78
17 59 0.54	-29 11 0.50	26.96	24.31	flat	...	1.05
17 58 58.37	-29 11 15.66	26.34	23.75	flat	...	0.63
17 59 4.34	-29 12 2.30	25.61	23.14	flat	...	0.32
17 59 3.17	-29 12 18.53	26.67	23.41	flat	...	0.96
17 59 5.10	-29 13 7.97	23.80	20.83	flat	...	0.11
17 59 2.92	-29 12 43.19	22.34	21.11	flat	...	0.04
17 59 4.61	-29 13 27.75	25.46	23.24	flat	...	0.32
17 59 1.35	-29 12 46.19	27.31	24.90	flat	...	1.23
17 59 6.88	-29 12 37.67	26.31	23.43	flat	...	0.61
17 59 0.31	-29 13 22.41	21.30	20.08	var/reg	6.44	0.04
17 58 54.60	-29 11 36.28	21.40	20.17	var/reg	0.13	0.07
17 58 57.40	-29 13 18.26	20.87	19.62	var/reg	1.49	0.10
17 58 59.00	-29 11 4.57	20.94	19.63	var/reg	1.35	0.06
17 58 58.07	-29 12 13.00	21.88	20.57	var/reg	1.92	0.14
17 58 54.06	-29 12 15.28	21.75	20.32	var/reg	0.79	0.11
17 58 54.88	-29 10 29.63	20.22	19.08	var/irreg	...	0.03
17 58 54.65	-29 12 11.71	20.18	18.94	var/reg	1.47	0.05
17 58 55.31	-29 11 28.88	20.82	19.70	var/irreg	...	0.04
17 58 59.25	-29 10 57.39	20.32	18.44	var/irreg	...	0.05
17 58 57.10	-29 12 58.73	20.99	19.80	var/reg	2.02	0.07
17 58 56.37	-29 12 54.06	22.41	20.77	var/reg	1.33	0.06
17 58 59.93	-29 11 55.12	20.09	18.94	var/irreg	...	0.04
17 58 53.74	-29 10 47.26	20.25	18.52	var/reg	2.75	0.05

Table A1—Continued

RA (J2000)	Dec (J2000)	V (F606W)	I) (F814W)	Variability Type	Period (d)	Range ^a
17 59 0.41	-29 11 44.32	21.93	20.53	var/irreg	...	0.10
17 58 55.17	-29 12 15.48	21.57	20.25	var/reg	1.72	0.07
17 58 55.14	-29 12 48.93	21.30	19.96	var/reg	7.03	0.05
17 58 53.09	-29 12 50.24	22.75	20.85	var/irreg	...	0.15
17 58 54.20	-29 12 29.68	20.06	18.86	var/irreg	...	0.04
17 58 55.98	-29 12 31.97	21.98	20.40	var/reg	2.32	0.11
17 58 56.88	-29 11 11.69	22.20	20.94	var/irreg	...	0.05
17 58 57.37	-29 10 40.02	22.17	20.81	var/reg	6.44	0.11
17 58 57.76	-29 12 8.28	20.45	19.27	var/reg	1.50	0.03
17 58 56.26	-29 13 36.83	21.38	19.99	var/reg	0.06	0.04
17 58 58.78	-29 10 49.51	22.60	20.94	var/reg	2.27	0.07
17 58 59.17	-29 10 21.82	21.64	20.19	var/reg	1.26	0.09
17 58 55.42	-29 13 9.91	24.34	22.33	var/reg	1.78	0.35
17 58 57.06	-29 13 35.16	20.58	19.35	var/irreg	...	0.09
17 58 57.21	-29 11 18.19	21.32	19.94	var/irreg	...	0.04
17 58 59.34	-29 10 35.30	21.78	20.31	var/reg	0.38	0.07
17 58 59.68	-29 13 14.44	22.33	20.65	var/reg	0.94	0.14
17 58 53.72	-29 13 28.78	24.02	22.22	var/reg	0.65	0.25
17 58 54.91	-29 10 30.76	20.01	18.73	var/irreg	...	0.06
17 58 55.71	-29 13 30.64	20.90	19.66	var/reg	2.44	0.09
17 58 54.44	-29 10 35.83	22.37	20.88	var/reg	4.81	0.10
17 58 55.79	-29 10 57.05	23.00	20.64	var/reg	2.84	0.19
17 58 54.17	-29 13 21.45	21.23	19.99	var/reg	2.09	0.05
17 58 54.90	-29 12 27.10	20.27	19.14	var/irreg	...	0.03
17 59 0.19	-29 11 32.85	23.06	20.34	var/reg	0.83	0.11
17 58 55.06	-29 13 12.33	23.95	21.98	var/reg	2.01	0.12
17 58 59.71	-29 12 17.19	22.55	21.05	var/reg	1.04	0.11
17 58 54.44	-29 11 45.74	22.34	20.93	var/reg	7.60	0.08
17 58 59.53	-29 10 29.80	20.10	18.75	var/irreg	...	0.09
17 58 57.20	-29 11 57.55	23.01	21.37	var/reg	0.38	0.16

Table A1—Continued

RA (J2000)	Dec (J2000)	V (F606W)	I) (F814W)	Variability Type	Period (d)	Range ^a
17 58 56.44	-29 11 13.40	23.25	21.51	var/reg	6.27	0.15
17 58 55.67	-29 10 56.72	25.68	24.40	var/reg	2.85	1.27
17 58 52.67	-29 13 32.92	21.63	19.85	var/irreg	...	0.12
17 59 2.88	-29 11 2.27	20.77	19.53	var/reg	1.60	0.09
17 59 1.11	-29 12 47.56	21.46	20.07	var/irreg	...	0.07
17 59 3.63	-29 13 19.71	22.35	19.96	var/irreg	...	0.06
17 59 7.09	-29 12 26.42	21.27	18.73	var/reg	1.10	0.04
17 59 5.64	-29 13 10.35	21.83	20.50	var/reg	1.98	0.09
17 59 1.13	-29 10 27.93	22.14	20.68	var/reg	0.90	0.07
17 59 7.54	-29 12 59.05	21.08	18.79	var/irreg	...	0.05
17 59 5.75	-29 10 57.46	20.01	18.87	var/irreg	...	0.03
17 59 3.66	-29 13 30.80	20.84	19.62	var/reg	5.95	0.05
17 59 1.33	-29 10 48.18	21.62	20.19	var/reg	1.29	0.10
17 59 7.17	-29 10 21.71	22.26	20.74	var/irreg	...	0.05
17 59 4.85	-29 11 15.24	22.05	20.33	var/reg	1.35	0.18
17 59 5.54	-29 10 44.69	21.44	20.14	var/reg	0.90	0.12
17 59 7.47	-29 13 22.25	22.22	19.97	var/reg	6.41	0.07
17 59 4.36	-29 13 7.39	21.18	19.90	var/reg	0.65	0.08
17 59 3.71	-29 11 56.65	20.16	19.05	var/reg	0.31	0.02
17 59 2.21	-29 10 51.44	20.98	19.67	var/irreg	...	0.05
17 59 3.80	-29 12 41.39	21.46	20.29	var/irreg	...	0.05
17 59 1.80	-29 13 24.95	21.48	20.28	var/reg	0.52	0.04
17 59 7.31	-29 10 55.30	20.08	18.96	var/reg	6.00	0.02
17 59 3.97	-29 13 11.61	23.14	21.50	var/reg	1.19	0.31
17 59 7.69	-29 12 38.15	23.41	21.70	var/reg	0.87	0.17
17 59 5.87	-29 13 18.64	22.24	20.56	var/reg	0.60	0.13
17 59 7.60	-29 13 8.61	20.14	19.01	var/irreg	...	0.03
17 59 7.99	-29 11 12.31	21.78	20.27	var/reg	1.22	0.10
17 59 8.41	-29 10 20.53	22.53	21.08	var/reg	1.66	0.14
17 59 4.22	-29 11 8.95	22.05	20.38	var/irreg	...	0.11

Table A1—Continued

RA (J2000)	Dec (J2000)	V (F606W)	I) (F814W)	Variability Type	Period (d)	Range ^a
17 59 8.49	-29 12 36.43	22.83	21.23	var/reg	2.78	0.13
17 59 3.37	-29 11 29.90	24.22	22.30	var/reg	0.71	0.19
17 59 4.86	-29 12 4.81	21.05	19.74	var/reg	1.18	0.06
17 59 7.02	-29 10 55.17	22.19	20.62	var/reg	0.61	0.15
17 59 5.47	-29 12 9.13	20.75	19.47	var/reg	0.85	0.08
17 59 2.63	-29 13 34.60	22.52	20.99	var/irreg	...	0.09
17 59 3.58	-29 10 59.49	21.77	20.30	var/reg	2.02	0.07
17 59 0.82	-29 12 30.11	22.41	20.92	var/reg	1.87	0.11
17 59 1.38	-29 12 58.27	22.91	21.32	var/irreg	...	0.20
17 59 6.17	-29 11 59.10	22.72	21.02	var/reg	2.84	0.10
17 59 5.17	-29 10 20.90	21.87	20.47	var/reg	0.84	0.10
17 59 4.23	-29 12 52.31	23.32	20.48	var/reg	0.66	0.13
17 59 7.00	-29 13 1.54	25.32	24.26	var/reg	11.79	0.77
17 59 4.73	-29 11 58.55	24.51	22.38	var/reg	1.54	0.29
17 59 4.47	-29 11 30.23	22.89	21.28	var/irreg	...	0.12

^aRange is defined as the difference in amplitude between the values in the 95th and 5th percentile in the original light curve; see §4.2 for details.

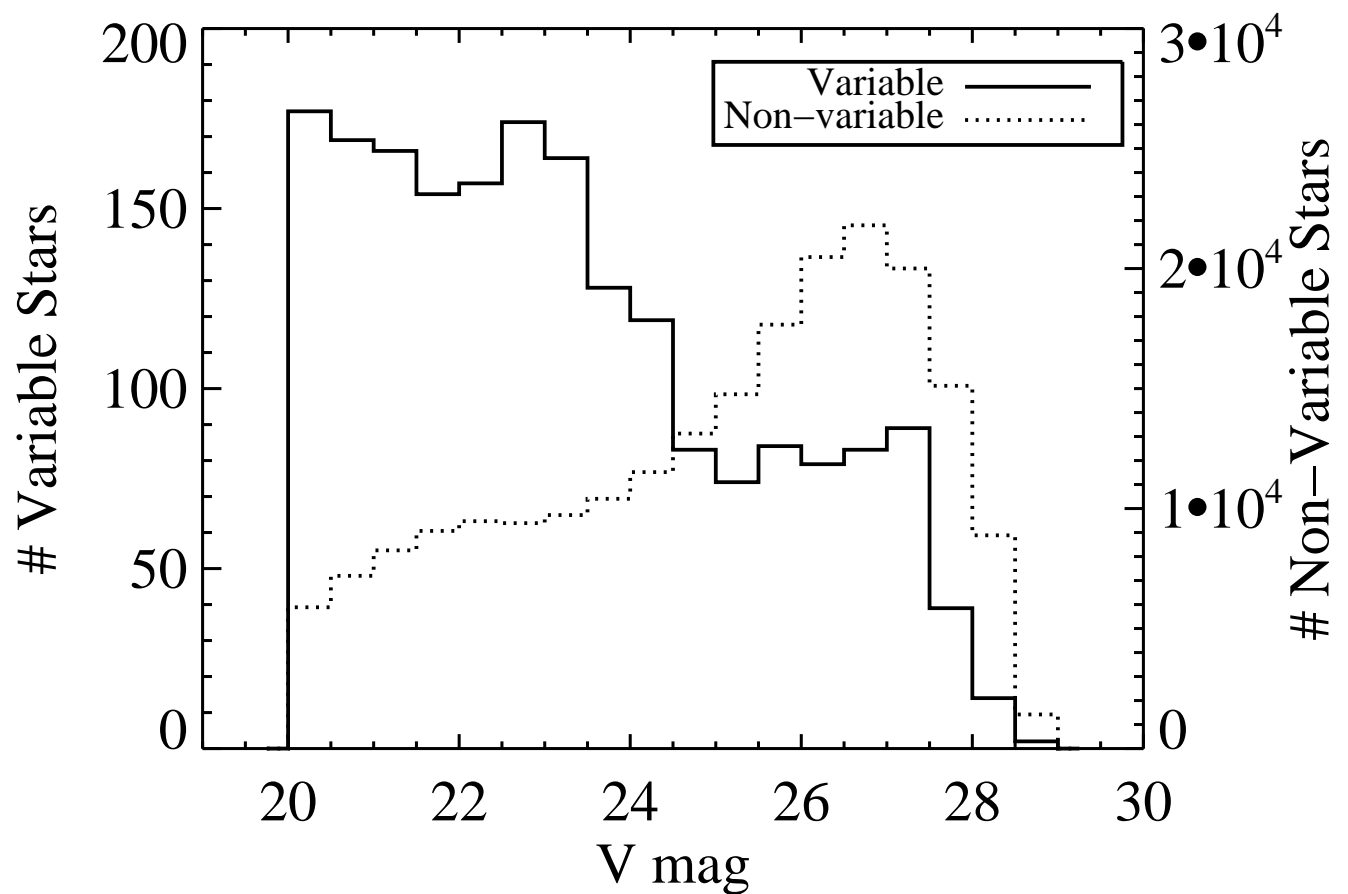


Fig. 1.— Plot of distribution of stars as a function of V_{F606W} magnitude, for stars deemed variable and non-variable, respectively. See §3.1 for discussion of sample division.

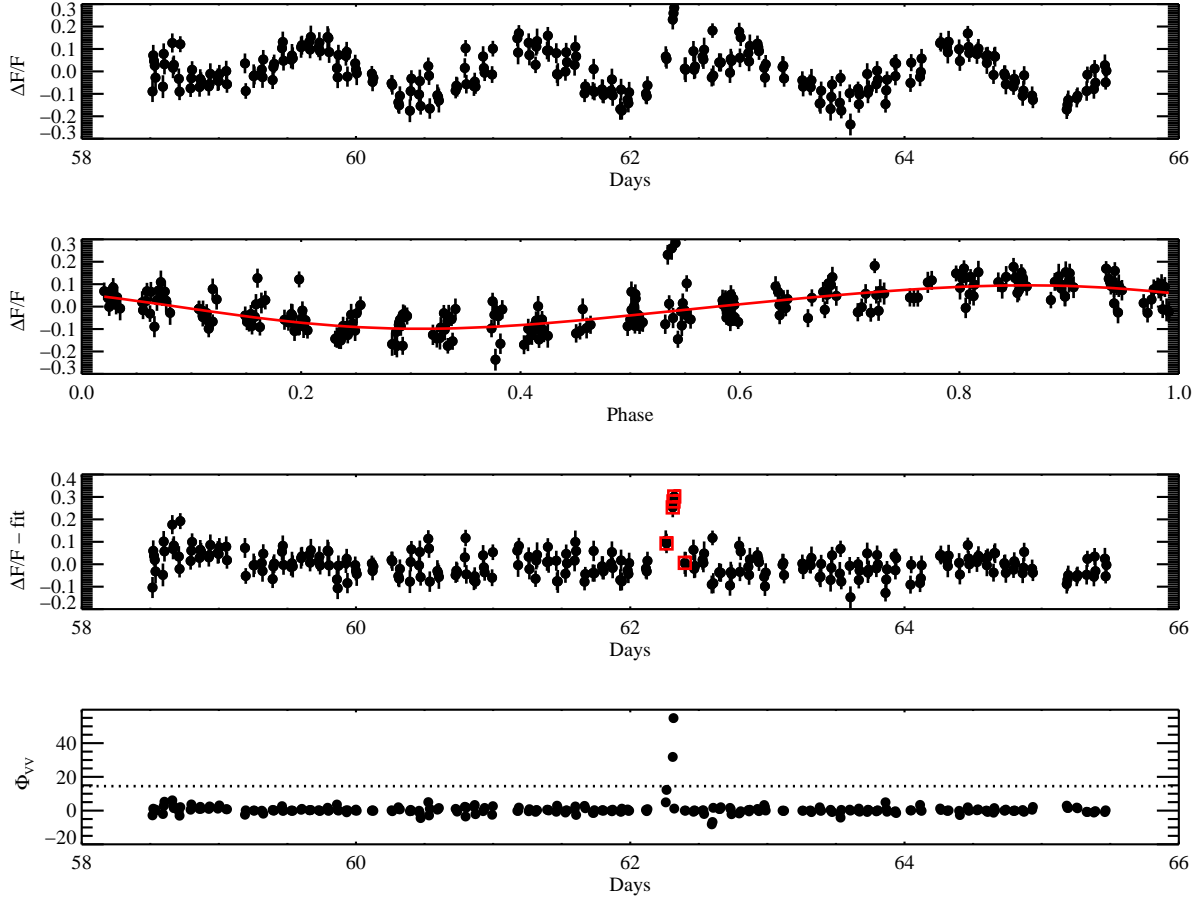


Fig. 2.— Example of a flare identified on a star with a variable light curve exhibiting regular periodic variations. Top panel shows relative fluxes versus time, and second panel from top shows the same data points, but folded over the best-fit period; the fit is shown in red. The third panel from the top shows the data after subtraction of the fit; red squares indicate time bins identified as a flare event. The bottom panel shows the ϕ_{VV} values for the detrended light curve. Only points which lie above the threshold value of $\phi_{VV}=14.5$ (dotted line in the bottom panel), have a value more than 2.5 times the standard deviation, and exhibit a positive increase are identified as flare peaks. The flare event (red squares in the third panel from the top) is constructed from data points adjacent to the flare peaks which have relative fluxes greater than zero. See §3.1 and §3.2 for more discussion.

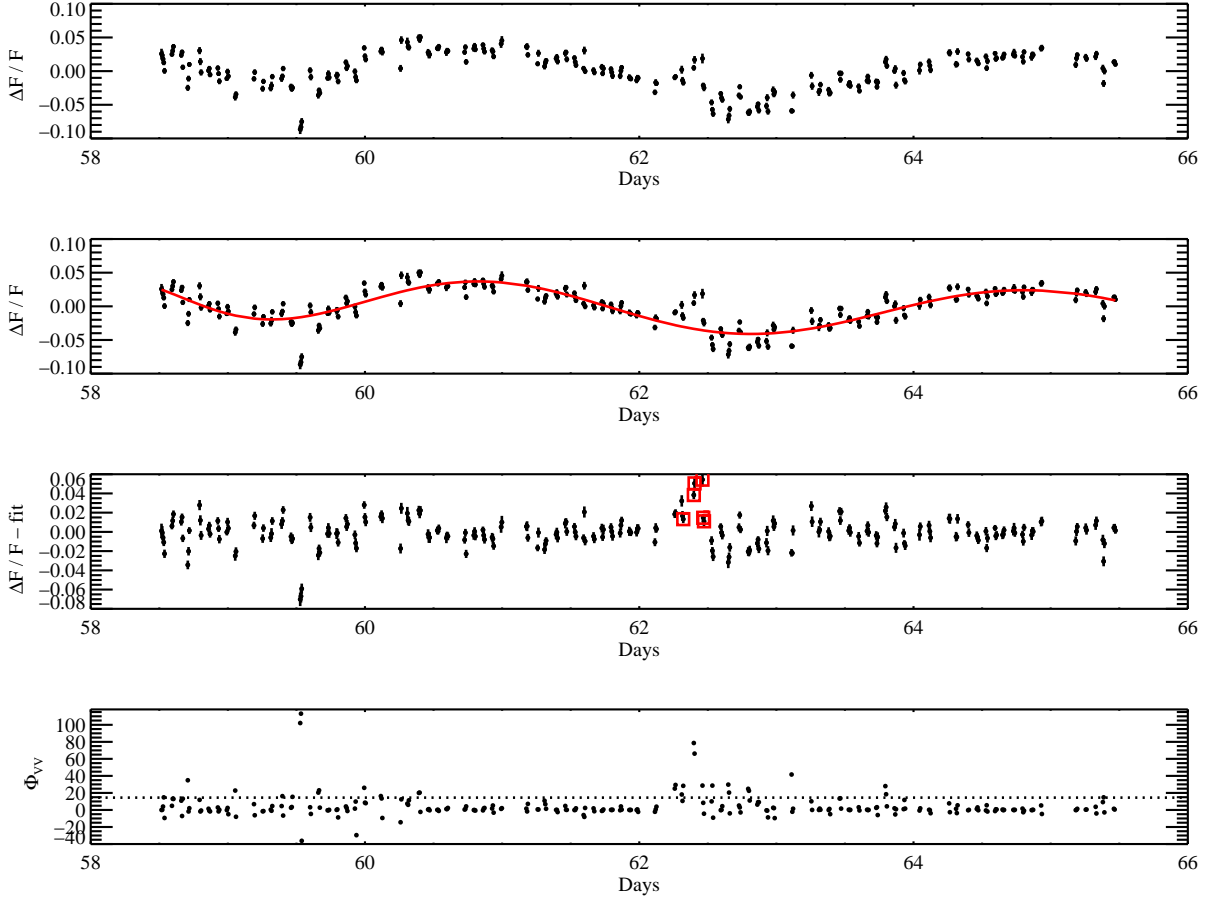


Fig. 3.— Example of a flare identified on a star with irregular variations. Panels are as in Figure 2. The irregularly variable stars may have varying amplitudes, such that when phase-folded over the dominant period these amplitudes don’t line up, or a changing slope to the rise of each light curve portion. In this example, the rise in amplitude from $t = 60 - 61$ is different than from $t = 63 - 65$, and the peak amplitudes are different. The fitting methods described in §3.1 are designed to detrend the light curve so that smaller scale temporal variations (flares) can be identified and studied. See §3.1 and §3.2 for more discussion.

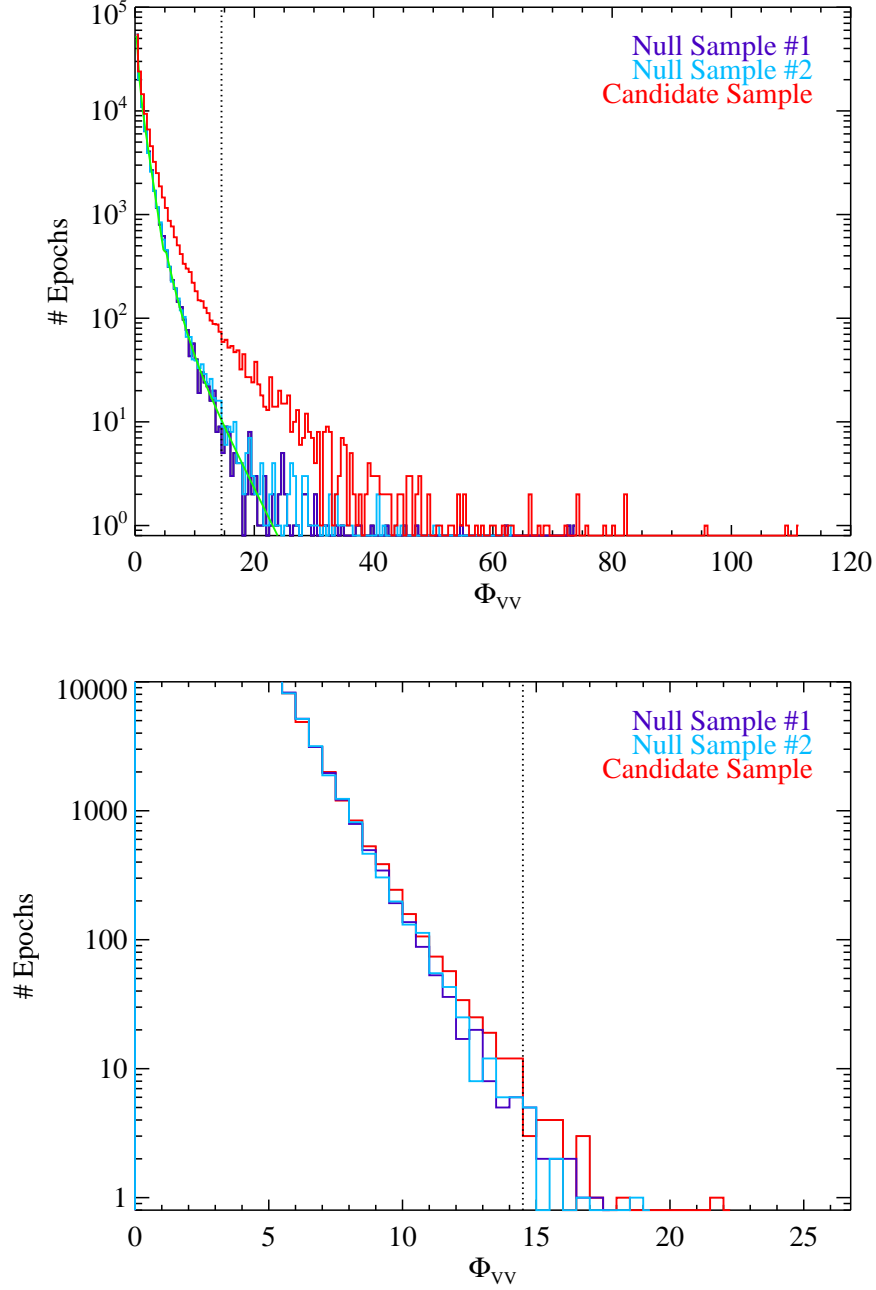


Fig. 4.— False discovery analysis of the variable sample (*top*) and non-variable sample (*bottom*). The null distributions (null samples #1 and #2) are epoch pairs with negative and positive flux changes (leading to negative ϕ_{VV} values – their absolute value is plotted here); the two null samples differentiate the ordering of the flux changes. The green curve in the top panel shows the sum of two Gaussians fitted to the null sample. The vertical dotted line indicates the cut-off value used to ensure a false discovery rate of 10%. See §3.2 for more discussion.

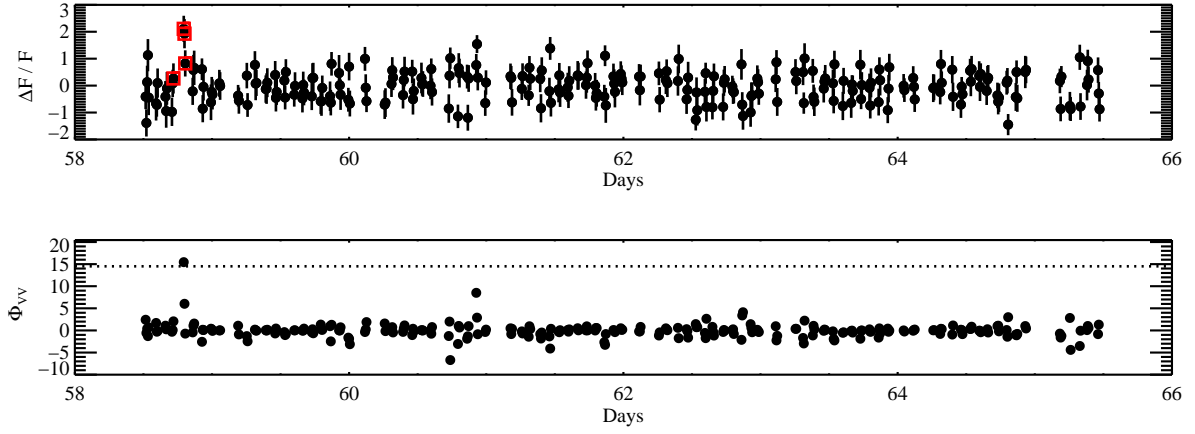


Fig. 5.— Light curve from a non-variable star, showing flare peak identification and points associated with a flare event. The top panel shows the relative flux variations as a function of time; the bottom panel shows the associated value of ϕ_{VV} calculated for each time bin. The dotted line in the bottom panel indicates the threshold above which peak flare events are identified. All points on either side of this identified flare peak which have relative fluxes greater than zero are included in the flare event. The red squares in the top panel indicate points identified as a flare event.

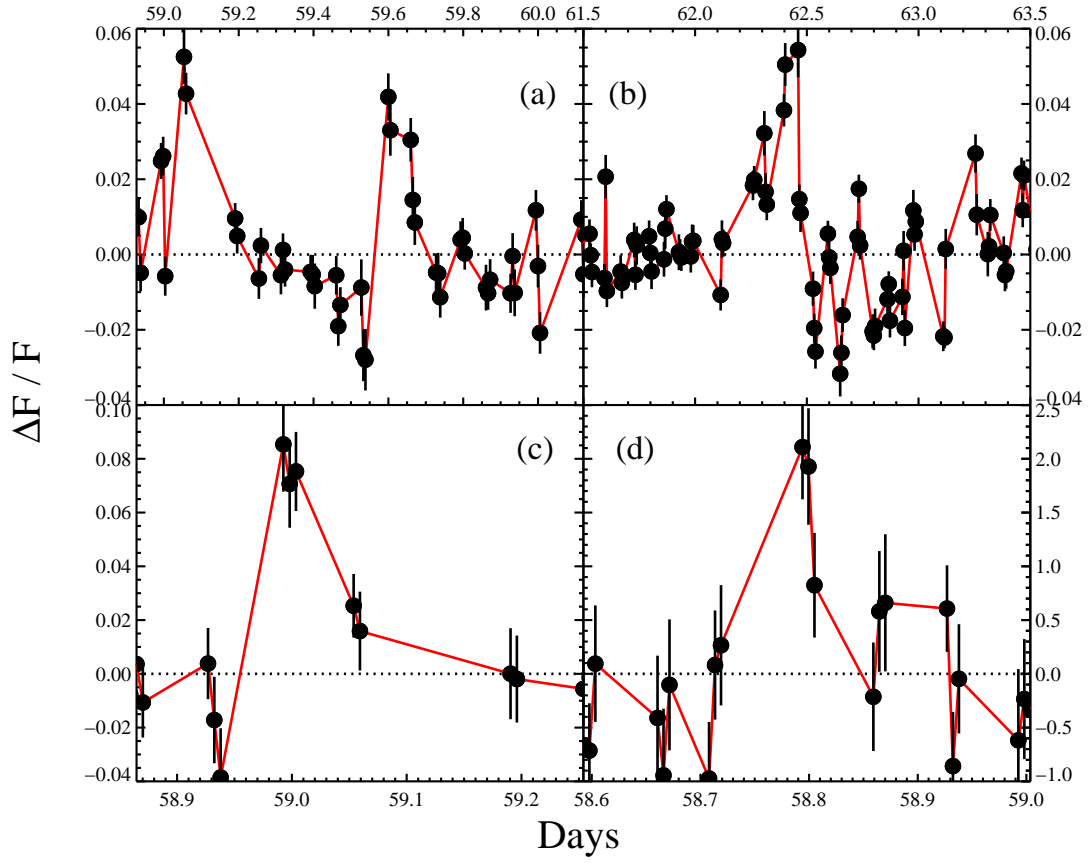


Fig. 6.— Close-up of five sample flares. Panels (a), (b), and (d) show flares which occurred on stars exhibiting underlying variability, and panel (c) depicts a flare seen on a non-variable star. Light curves on variable stars have been detrended, as described in §3.1. Panel (a) shows two flares on the same star while panel (b) shows a complex flare event.

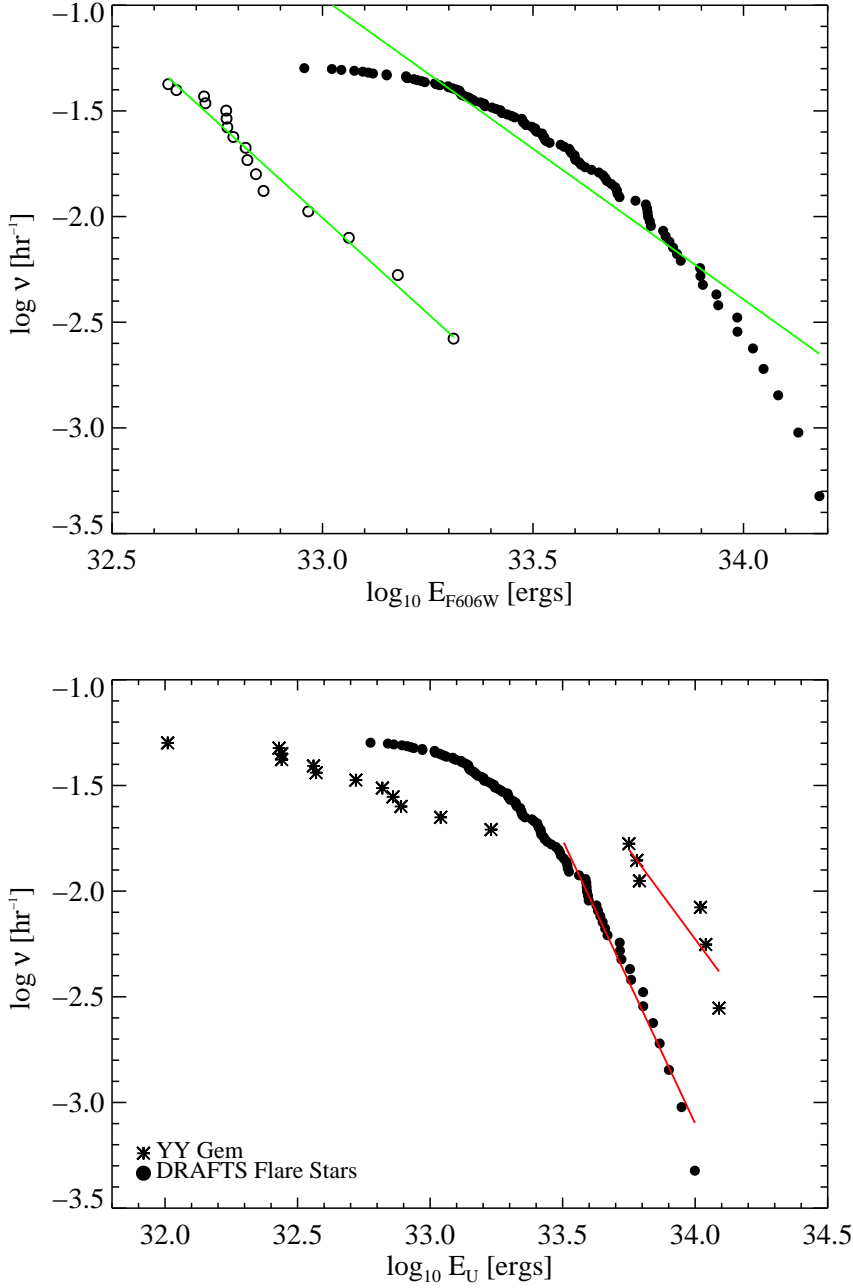


Fig. 7.— (*top*) Frequency of stellar flares as a function of flare energy, for flares occurring on non-variable stars (open circles) and variable stars (filled circles). The computation of quantities is described in §4.1. Green lines indicate fits to the flare frequency distributions, the parameters of which are listed in Table 2. (*bottom*) Flare frequency distribution of variable stars after conversion to an equivalent U-band flare energy (filled circles), and compared to the flare frequency distribution of the well-studied cool dwarf binary YY Gem (asterisks), using the observations of Lacy et al. (1976). The red lines show fits to the distribution above an energy of $10^{33.5}$ erg, corresponding to a break in the distribution of flare energies for YY Gem (Doyle & Mathioudakis 1990) and to a roll over in the distribution of DRAFTS variable stars.

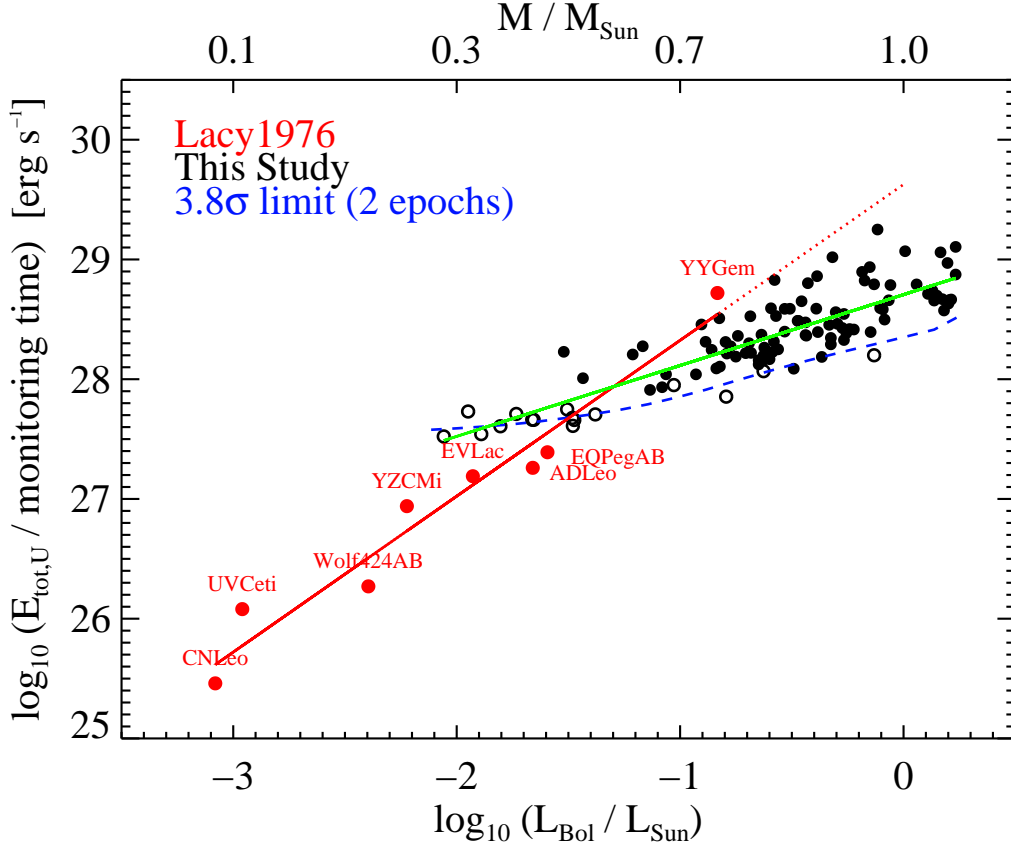


Fig. 8.— The energy loss rate due to flares plotted against stellar bolometric luminosity, for each star identified as a flare star. The calculation of quantities is discussed in §4.1. Filled black circles represent results for variable DRAFTS flare stars, while open circles show results for non-variable DRAFTS flare stars. Red filled circles are results from Lacy et al. (1976) for a sample of M dwarf flare stars. The blue dashed line indicates the approximate limit based on 3.8σ detections at two epochs, which gives the cutoff value ϕ_{VV} of 14.5. The deviation per epoch was used to get a limiting relative flux. A fit to the trend of flare energy loss rate vs stellar luminosity is shown for all DRAFTS stars in green, and the red line illustrates a fit to the dMe stars in Lacy et al. (1976), extrapolated to $L_{\text{bol}}=L_{\text{sun}}$. The axis at the top of the plot lists conversion between stellar bolometric light and mass using the bulge isochrone, and is only appropriate for single stars. The average energy loss rate for the flaring stars identified here far exceeds all of the M dwarf flare stars studied in Lacy et al. (1976) except for the close binary YY Gem, although the steeper trend of the dMe stars would imply a larger energy loss rate at $L_{\text{bol}}=L_{\text{sun}}$.

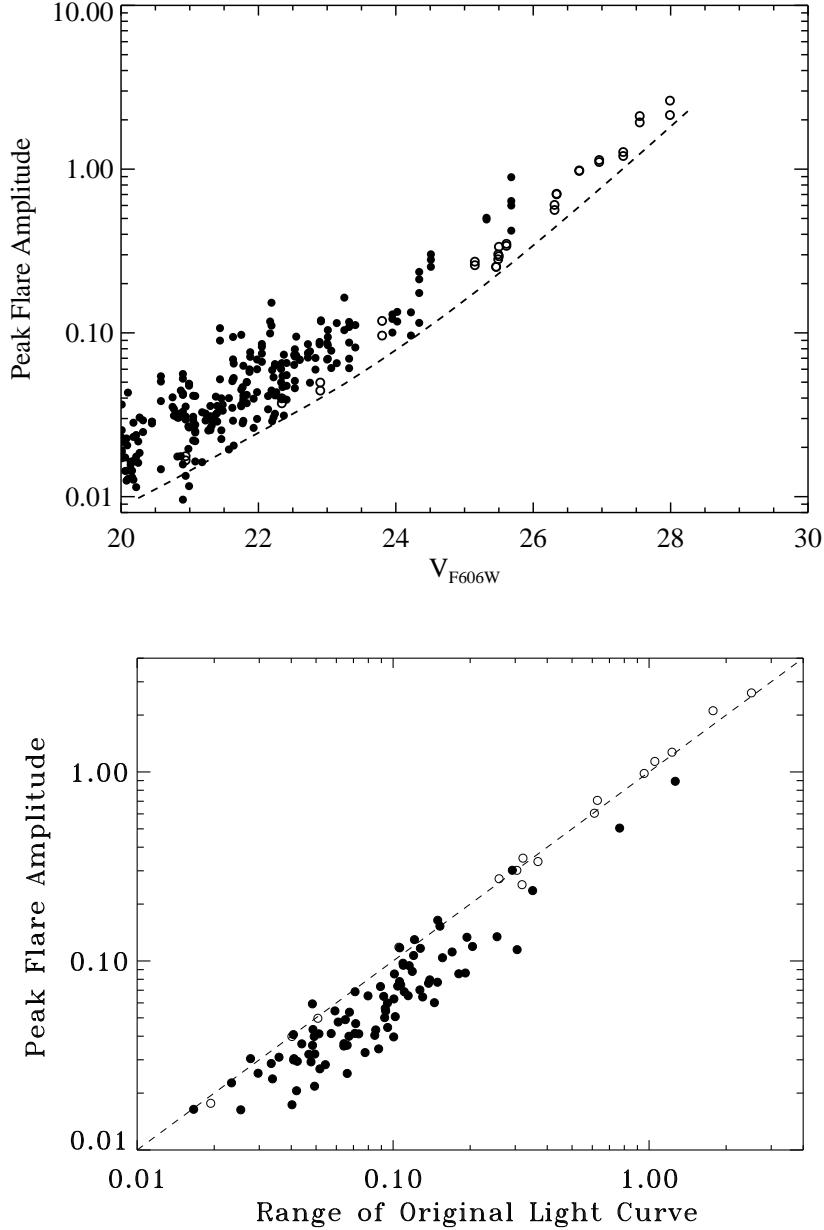


Fig. 9.— (*top*) Plot of peak flare amplitude as a function of V_{F606W} of the star, for flares identified through selective filtering of the time series. Filled circles represent flares on variable stars, and open circles flares on non-variable stars. The dotted line represents the noise level given by Poisson statistics for a star of a given magnitude. In general, the statistics on the brighter stars enabled identification of flares with increases of a few tens of percent, while for the fainter stars only larger variations could be detected. (*bottom*) Plot of the peak flare amplitude versus the range of the star’s light curve, defined as the difference in amplitude between the 95th and 5th percentiles, for all flaring stars. Symbols are as in the top panel. The dashed line indicates a line of equality. For stars with multiple flares, the peak flare amplitude is the amplitude of the largest flare. There is strong correlation between the range of underlying variability and flare amplitudes in this sample of stars.

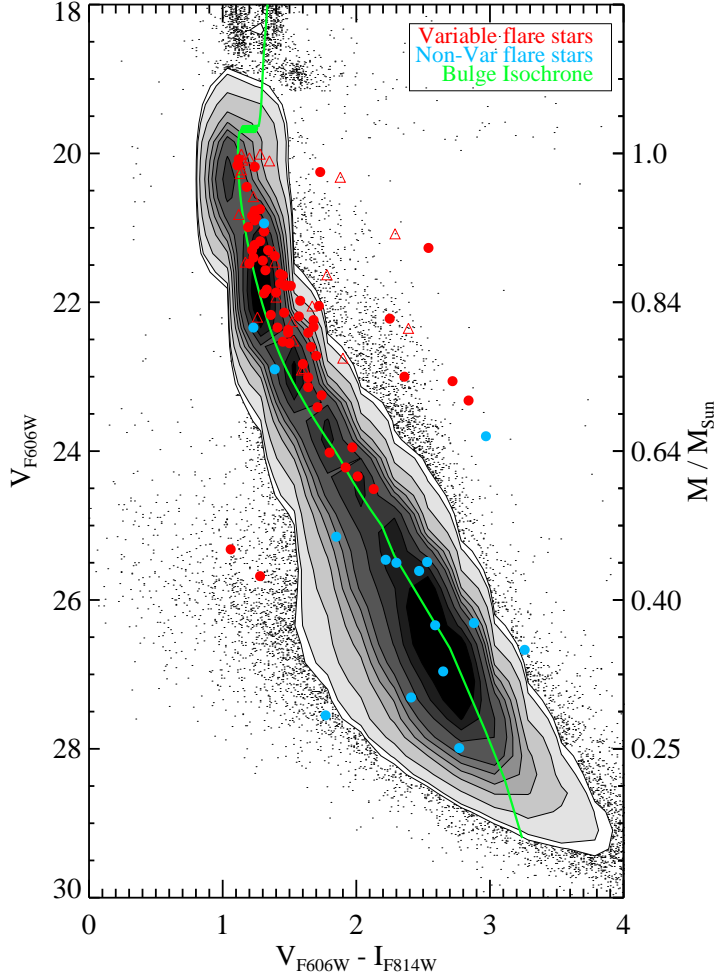


Fig. 10.— Color-magnitude diagram (CMD) for all stars in the SWEEPS dataset. Small black dots give location of individual stars where density of points is low; otherwise shaded contours are displayed. The green line gives a bulge isochrone appropriate for a 10 GY stellar population, with distance modulus $(m - M)_0 = 14.3$, foreground extinction $E(B - V) = 0.64$, solar metallicity, and $[\alpha/\text{Fe}] = 0.3$. Red symbols display the locus of variable flare stars on the CMD, while blue circles illustrate the location of non-variable flare stars. Regularly variable stars are indicated with a filled circle, while the irregularly variable ones are shown with a hollow triangle. The axis on the right side of the figure gives the appropriate mapping between luminosity and mass, using the bulge isochrone in green.

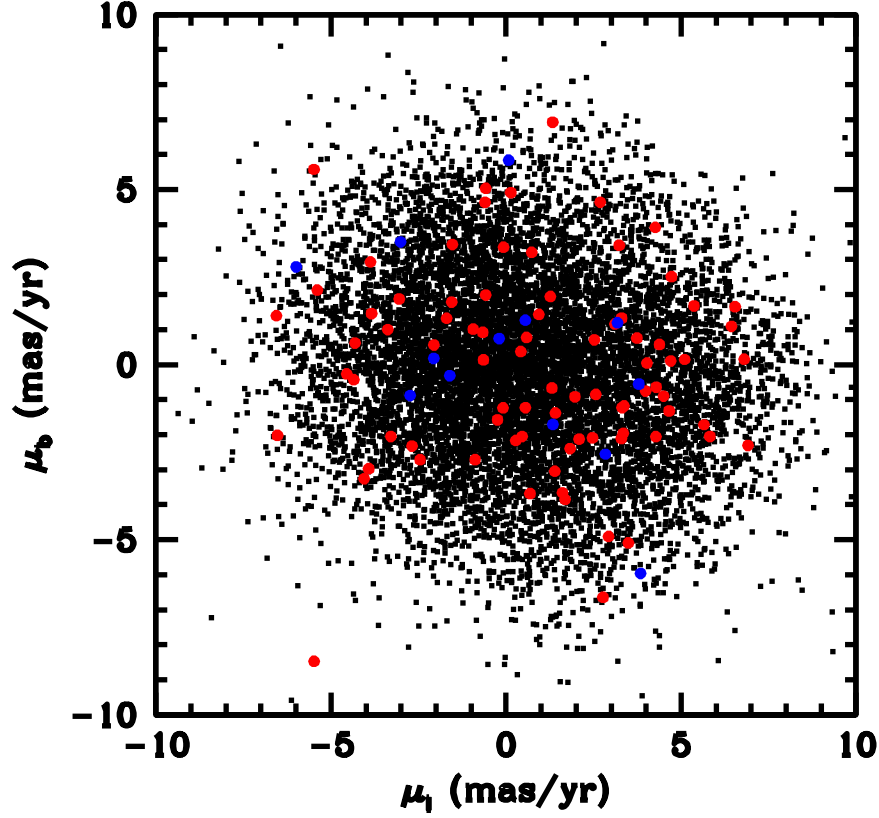


Fig. 11.— Distribution of proper motions in galactic latitude (μ_l) and longitude (μ_b) for stars in the SWEEPS field. The black dots show the locations of 20,000 random stars in the SWEEPS field, while the red and blue points show the values of variable and non-variable flaring stars, respectively, which had proper motion measurements (as described in Clarkson et al. 2008). There does not appear to be any tendency for the flaring stars to have a different distribution than the bulge stars.

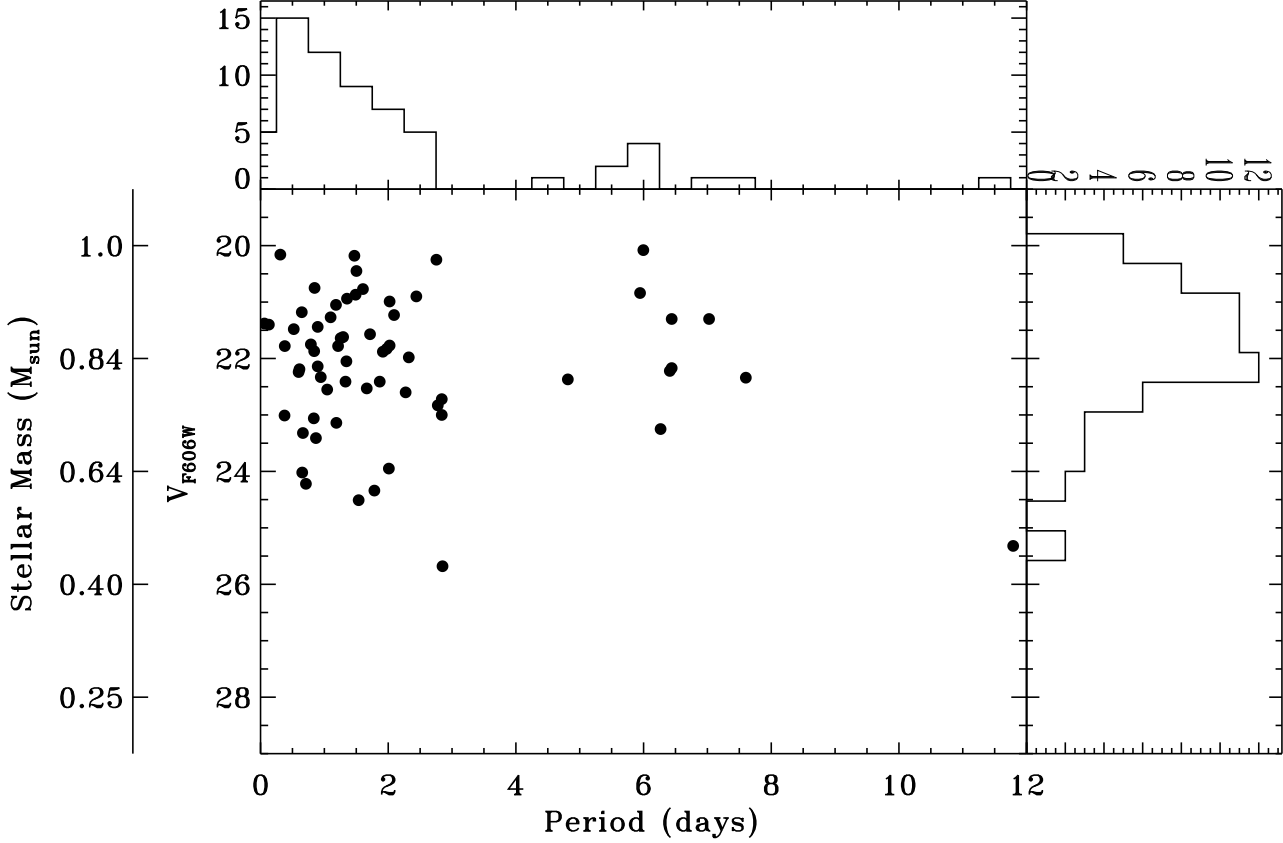


Fig. 12.— Star’s V_{F606W} versus period for the 63 flaring stars exhibiting regular periodic variations. Most (84%) of these flaring stars have periods less than 3 days. The relative number of variable stars drops for $V > 24.5$ (as indicated from Figure 1) reflecting our inability to establish these underlying variations. For brighter stars there does not appear to be any bias in the stellar brightness versus period. The conversion between stellar magnitude and mass is shown on the axis to the left, using the bulge isochrone of Sahu et al. (2006); this is only appropriate for single stars.

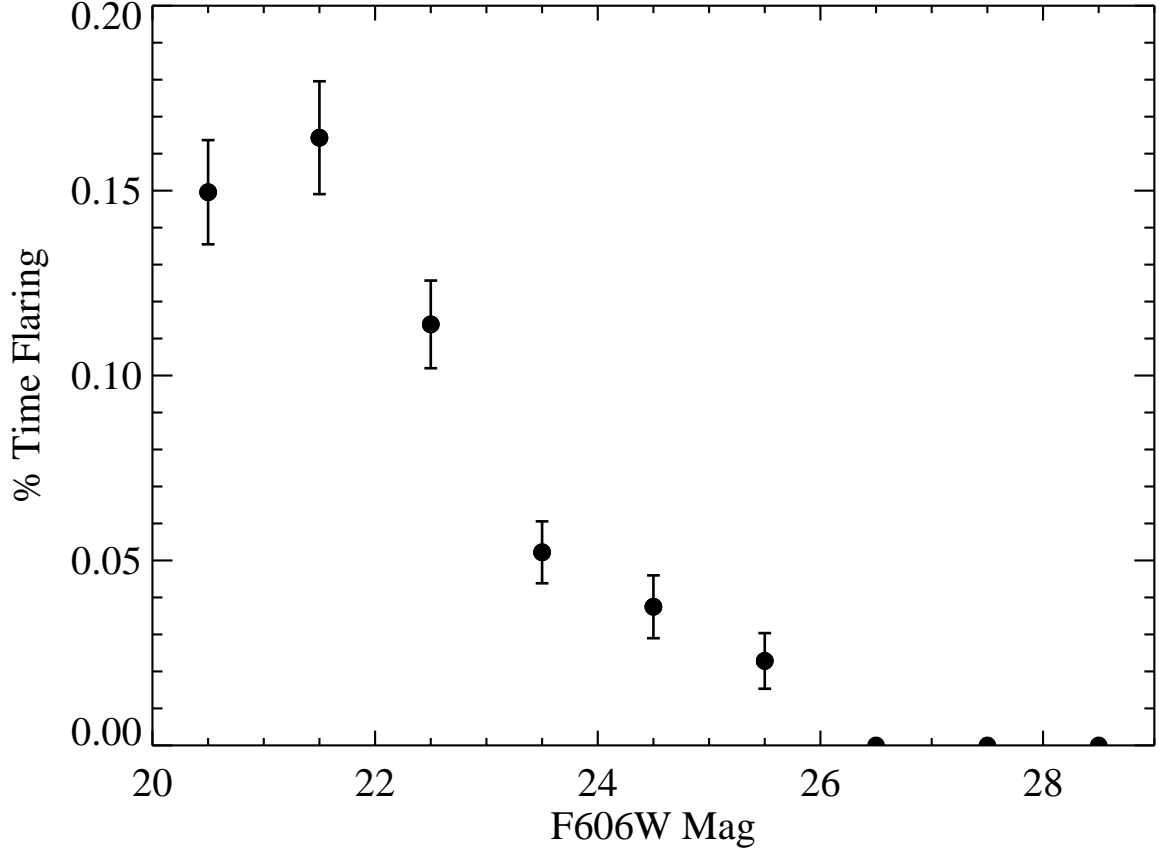


Fig. 13.— Variation of the fraction of epochs affected by flaring against stellar magnitude, for all variable stars. Percentages were computed by summing the number of epochs in a given magnitude bin which were identified as a flare by our algorithm, and dividing by the total number of epochs in that magnitude bin. For fainter stars our ability to detect flares becomes more difficult.